RESEARCH ARTICLE SUMMARY

NEUROSCIENCE

Meissner corpuscles and their spatially intermingled afferents underlie gentle touch perception

Nicole L. Neubarth*, Alan J. Emanuel*, Yin Liu*, Mark W. Springel, Annie Handler, Qiyu Zhang, Brendan P. Lehnert, Chong Guo, Lauren L. Orefice, Amira Abdelaziz, Michelle M. DeLisle, Michael Iskols, Julia Rhyins, Soo J. Kim, Stuart J. Cattel, Wade Regehr, Christopher D. Harvey, Jan Drugowitsch, David D. Ginty†

INTRODUCTION: Meissner corpuscles are mechanosensory end organs that densely occupy mammalian glabrous skin. The basic anatomy of the Meissner corpuscle and the Aβ (large soma diameter and fast action potential conducting) mechanosensory neurons that innervate it have been widely described. However, little is known about the requirement for the Meissner corpuscle and its innervating Aβ mechanosensory neurons for touch-related behaviors, sensorimotor capabilities, and tactile perception.

RATIONALE: Mice lacking either brain-derived neurotrophic factor (BDNF) or its receptor TrkB have a range of developmental deficits, including an absence of Meissner corpuscles. We reasoned that confining TrkB manipulations to sensory neurons in conjunction with selective genetic labeling approaches would allow us to investigate the developmental assembly of Meissner corpuscles and their functions in somatosensation. While examining Meissner corpuscle development, we found that two Aβ mechanosensory neuron types innervate the corpuscle. Here, we assessed the requirement of Meissner corpuscles for touch sensitivity and fine sensorimotor control and the anatomical, physiological, and ultrastructural properties of the two Aβ sensory neurons that innervate this mechanosensory end organ.

Meissner corpuscles are required for perception of gentle touch and fine sensorimotor control

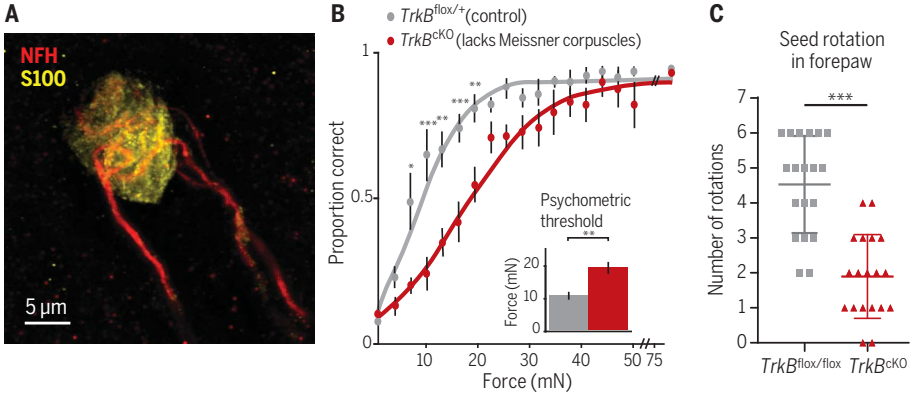

Two molecularly and physiologically distinct Aβ neurons innervate Meissner corpuscles and differentially associate with corpuscle lamellar cells

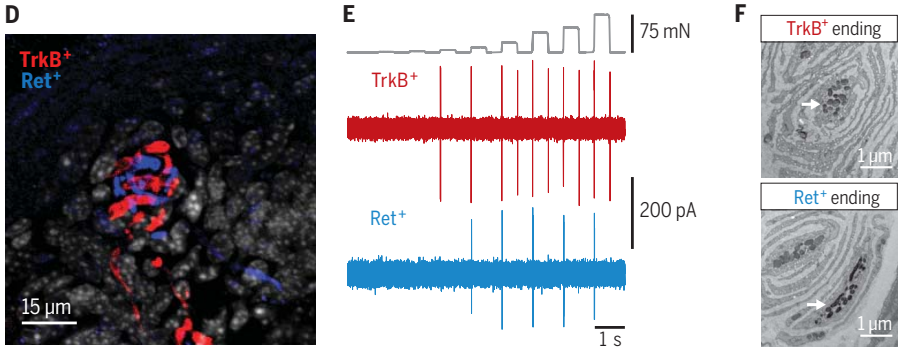

Anatomy and physiology of Meissner corpuscles required for tactile behavior. (**A** to **C**) Meissner corpuscles and their Aβ afferents (A) were required for normal tactile sensitivity (B) and fine sensorimotor control (C). (**D**) TrkB$^+$ and Ret$^+$ Aβ neurons both innervated Meissner corpuscles. (**E** and **F**) TrkB$^+$ Meissner afferents were more sensitive (E) and had more lamellar cell wrappings [(F), arrows indicate axons wrapped with lamellar processes] compared with Ret$^+$ Meissner afferents. In (A), S100 and NFH are antibodies used to visualize Meissner corpuscles and their afferents, respectively. In (B) and (C), error bars represent SEM, and *p < 0.05, **p < 0.01, and ***p < 0.001.

RESULTS: Sensory neuron–specific knockout of TrkB resulted in complete loss of Meissner corpuscles without affecting other mechanosensory end organs in mouse glabrous (nonhairy) skin, including Aβ mechanosensory neuron–Merkel cell complexes and Pacinian corpuscles. Behavioral measurements showed that mice lacking Meissner corpuscles were deficient in perceiving and reacting to the gentlest detectable forces acting on glabrous skin and in fine sensorimotor control.

ON OUR WEBSITE

Read the full article at https://dx.doi.org/10.1126/science.abb2751

Genetic labeling experiments revealed that Meissner corpuscles are innervated by two molecularly distinct Aβ sensory neuron types, one that expresses TrkB and the other that expresses the tyrosine kinase Ret. Despite innervating the same end organ, the responses of these two Aβ neuron types to tactile stimuli differed: The TrkB-positive (TrkB$^+$) Meissner afferent was more sensitive and responded at both the onset and the offset of step indentations of glabrous skin, whereas the Ret$^+$ Meissner afferent was less sensitive and rarely responded at step offset. Some Ret$^+$ neurons even had sustained responses during a static indentation stimulus. In addition, the axonal endings of these two Aβ mechanosensory neuron types were found to be homotypically tiled but heterotypically offset. Computational modeling suggested that this anatomical arrangement maximizes information available for encoding acuity while ensuring complete coverage of the skin using a limited number of neurons. Finally, ultrastructural analysis using electron microscopy revealed that the axon terminals of the more sensitive TrkB$^+$ Meissner afferents had greater numbers of lamellar cell wrappings than the terminals of the less sensitive Ret$^+$ Meissner afferents.

CONCLUSION: We conclude that two homotypically tiled but heterotypically offset Aβ mechanosensory neurons with distinct molecular, physiological, and ultrastructural properties innervate Meissner corpuscles, which underlie the perception of, and behavioral responses to, the gentlest detectable forces acting on glabrous skin. ■

The list of author affiliations is available in the full article online.
*These authors contributed equally to this work.
†Corresponding author. Email: david_ginty@hms.harvard.edu
Cite this article as N. L. Neubarth *et al.*, *Science* **368**, eabb2751 (2020). DOI: 10.1126/science.abb2751

RESEARCH ARTICLE

NEUROSCIENCE

Meissner corpuscles and their spatially intermingled afferents underlie gentle touch perception

Nicole L. Neubarth[1,2]*†, Alan J. Emanuel[1,2]*, Yin Liu[3,4]*, Mark W. Springel[1,2], Annie Handler[1,2], Qiyu Zhang[1,2], Brendan P. Lehnert[1,2], Chong Guo[1], Lauren L. Orefice[1,2], Amira Abdelaziz[1,2], Michelle M. DeLisle[1,2], Michael Iskols[1,2], Julia Rhyins[1,2], Soo J. Kim[1,2], Stuart J. Cattel[1,2], Wade Regehr[1], Christopher D. Harvey[1], Jan Drugowitsch[1], David D. Ginty[1,2]‡

Meissner corpuscles are mechanosensory end organs that densely occupy mammalian glabrous skin. We generated mice that selectively lacked Meissner corpuscles and found them to be deficient in both perceiving the gentlest detectable forces acting on glabrous skin and fine sensorimotor control. We found that Meissner corpuscles are innervated by two mechanoreceptor subtypes that exhibit distinct responses to tactile stimuli. The anatomical receptive fields of these two mechanoreceptor subtypes homotypically tile glabrous skin in a manner that is offset with respect to one another. Electron microscopic analysis of the two Meissner afferents within the corpuscle supports a model in which the extent of lamellar cell wrappings of mechanoreceptor endings determines their force sensitivity thresholds and kinetic properties.

The basic anatomy of the Meissner corpuscle and its presumed innervating Aβ rapidly adapting type I (RAI) low-threshold mechanoreceptor (LTMR) have been widely described since its discovery in 1852 (*1*). However, the Meissner corpuscle's requirement for touch-related behaviors, sensorimotor capabilities, and tactile perception have remained a matter of speculation.

Results

BDNF signaling is required for Meissner corpuscle development

Mice lacking either brain-derived neurotrophic factor (BDNF) or its receptor TrkB die neonatally and notably also have a complete absence of Meissner corpuscles (*2*–*4*). We thus generated conditional mutant mouse models that are viable in adulthood and selectively lack Meissner corpuscles for addressing their role in tactile perception and sensorimotor behaviors in adult animals. We found that BDNF is expressed in glabrous skin during the period of Meissner corpuscle formation (fig. S1, A to C). Eliminating BDNF expression in epithelial cells of the skin using *K5Cre; BDNF*$^{flox/flox}$ mice resulted in a dramatic reduction in the number of Meissner corpuscles (fig. S1, F to H). We found no disturbance of Meissner corpuscles in mice lacking BDNF in neurons of the dorsal root ganglia (DRG) or Schwann cells (*Wnt1*^{Cre}*; BDNF*$^{flox/flox}$; fig. S1, D, E, and H), suggesting that skin-derived, and not neuron- or Schwann cell–derived, BDNF is crucial for Meissner corpuscle development. BDNF's cognate receptor, TrkB, is present in a subset of primary sensory neurons of the DRG, and mice that selectively lack TrkB in primary sensory neurons (*Advillin*^{Cre}*; TrkB*$^{flox/flox}$, hereafter called *TrkB*^{cKO}) (*5*, *6*), although viable and overtly normal, are also devoid of Meissner corpuscles and their innervating sensory neurons (Fig. 1, A and B, and fig. S2). Mice that lack TrkB in Schwann cells, on the other hand, have a normal complement of Meissner corpuscles (fig. S2, H and J). Although some neurofilament-positive (NFH$^+$) sensory fibers were present in glabrous skin dermal papillae of *TrkB*^{cKO} mice before postnatal day 20 (P20), these fibers were absent in adults (Fig. 1A and fig. S2). By contrast, Merkel cells and the cutaneous endings of their associated Aβ slowly adapting (SA) LTMRs, which are TrkB-negative, were found in comparable numbers in glabrous skin of control and *TrkB*^{cKO} adult mice (Fig. 1, A and B). We next did in vivo loose-patch electrophysiological recordings (*7*, *8*) of random L4 DRG neurons from adult control and *TrkB*^{cKO} mice. Whereas indentation of hindpaw glabrous skin with gentle force steps evoked both Aβ RA-LTMR and Aβ SA-LTMR physiological responses in control mice, Aβ RA-LTMR responses were absent in *TrkB*^{cKO} mice even at indentation forces as high as 75 mN (Fig. 1, D to F). Activation thresholds and firing patterns of Aβ SA-LTMRs in control and *TrkB*^{cKO} mice were indistinguishable (Fig. 1G). Thus, BDNF and TrkB expressed in glabrous skin epithelial cells and sensory neurons of the DRG, respectively, are essential for development of Meissner corpuscles and the presence of Aβ RA-LTMR responses to indentation of glabrous skin. By contrast, sensory-neuron TrkB signaling is dispensable for the development and normal response properties of Merkel cells and their associated Aβ SA-LTMRs and, as found previously, the development of Pacinian corpuscles (*2*–*4*, *9*).

Meissner corpuscles are required for normal glabrous skin sensitivity

We subjected adult control and *TrkB*^{cKO} mice to behavioral tests of glabrous skin sensitivity, light touch perception, gait analysis, and fine sensorimotor control. First, we measured glabrous hindpaw withdrawal thresholds in *TrkB*^{cKO} and littermate control mice using forces ranging from 0.008 to 4.0 g applied to the pedal pads of the hindpaw (Fig. 2A). Wild-type mice withdrew their paws in response to the entire range of forces presented, rarely reacting to the lowest forces and nearly always reacting to the highest forces. On the contrary, although *TrkB*^{cKO} mice displayed normal hindpaw withdrawal at the high end of this force range, they were unresponsive to the lightest forces (Fig. 2A). We infer from these behavioral measurements that activation of Merkel cell complexes and Aβ SA-LTMRs does not underlie sensorimotor responses to the lightest detectable forces acting on glabrous skin. To further test whether this deficit was specific to disruption of Meissner corpuscles and not to disturbance of Merkel cell complexes, we measured withdrawal thresholds in mice lacking Merkel cells (*K5Cre*; *Atoh1*$^{flox/flox}$ or *Atoh1*^{cKO}) (*10*–*16*). In mice lacking Merkel cells, Meissner corpuscles were present in slightly increased numbers (Fig. 1C). Behaviorally, mice lacking Merkel cells performed normally on the von Frey paw withdrawal test (Fig. 2B).

Next, we trained water-deprived mice within an operant conditioning behavioral paradigm to report detection of glabrous skin indentation stimuli by lick retrieval of a water reward (Fig. 2, C to E). Mice learned to lick specifically in response to mechanical stimuli within 2 weeks, at which time we delivered step indentations ranging between 0 and 75 mN to the forepaw and measured perceptual detection thresholds (force at the midpoint of the psychometric function; Fig. 2F). Whereas control mice exhibited perceptual detection thresholds of about 10 mN, mice lacking Meissner corpuscles had increased perceptual thresholds of about 20 mN. By contrast, reactivity to a light air puff applied to back hairy skin was comparable in control and *TrkB*^{cKO} mice (fig. S3), indicating normal hairy skin sensitivity.

Meissner corpuscles are required for normal fine sensorimotor behavior

We next tested the requirement of Meissner corpuscles in an innate, fine sensorimotor

[1]Department of Neurobiology, Harvard Medical School, 220 Longwood Avenue, Boston, MA 02115, USA. [2]Howard Hughes Medical Institute, Harvard Medical School, 220 Longwood Avenue, Boston, MA 02115, USA. [3]Department of Biochemistry, Stanford University, 279 Campus Drive, Stanford, CA 94305, USA. [4]Howard Hughes Medical Institute, Stanford University, 279 Campus Drive, Stanford, CA 94305, USA.
*These authors contributed equally to this work.
†Present address: Two Six Labs, 901 North Stuart Street, Arlington, VA 22203, USA.
‡Corresponding author. Email: david_ginty@hms.harvard.edu

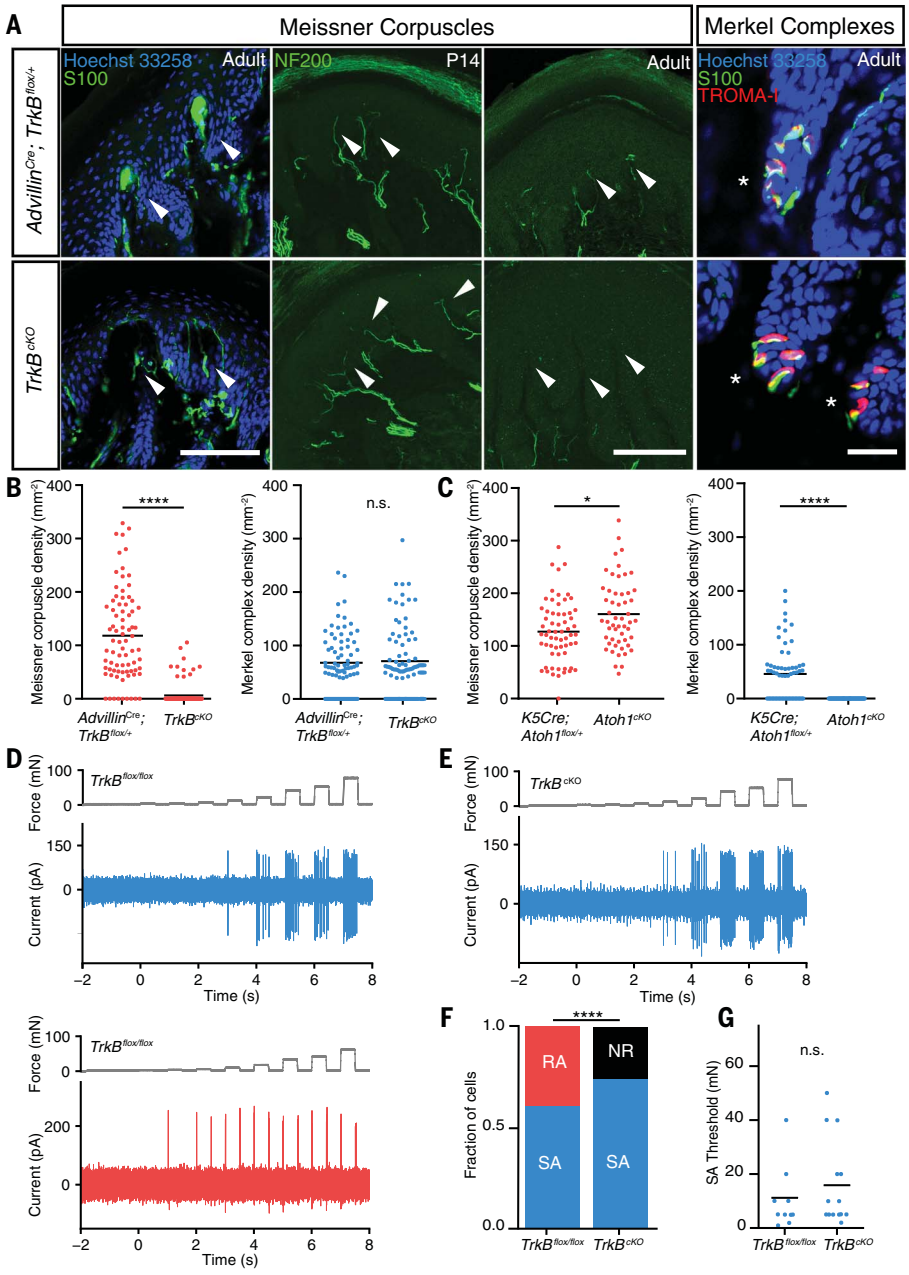

Fig. 1. Meissner corpuscles and their innervating Aβ LTMRs are absent in *TrkB*^{cKO} mice. (**A**) Digital pad sections from control (top) and *TrkB*^{cKO} mice (bottom). Arrows and asterisks indicate typical locations of Meissner corpuscles and Merkel complexes, respectively. Meissner corpuscles and their afferents are labeled with S100 or NFH immunostaining in separate sections, respectively (scale bars, 100 μm). Merkel cells and associated nerve terminals are labeled with TROMA-I and S100, respectively (scale bar, 25 μm). (**B**) Meissner corpuscle and Merkel complex density in glabrous pads of control and *TrkB*^{cKO} mice. Dots represent individual sections, and black bars represent mean [79 sections from three control mice and 81 sections from three *TrkB*^{cKO} mice; two-tailed Mann-Whitney *U* test, ****$p < 0.0001$ ($U = 580$), n.s. indicates not significant ($U = 3163$, $p = 0.9016$)]. (**C**) Meissner corpuscle and Merkel complex density in pads of *K5Cre; Atoh1*$^{flox/+}$ and *Atoh1*^{cKO} (*K5Cre; Atoh1*$^{flox/flox}$) mice. Dots represent densities from individual sections, and black bars represent means [62 sections from two *K5Cre; Atoh1*$^{flox/+}$ mice and 53 sections from two *Atoh1*^{cKO} mice; two-tailed Mann-Whitney *U* test, *$p = 0.0113$ ($U = 1193$), ****$p < 0.0001$ ($U = 689$)]. (**D**) In vivo recordings of a SA (top, blue) and a RA (bottom, red) Aβ LTMR from control mice in response to step indentations applied to glabrous hindpaw pedal pads (force records shown in gray). (**E**) Example recording of an Aβ SA-LTMR from a *TrkB*^{cKO} mouse in response to the same stimulus as in (D). (**F**) Proportion of neurons that are SA, RA, and not responsive (NR) to indentation in control (left, $n = 18$ cells) and *TrkB*^{cKO} mice (right, $n = 20$ cells). χ^2 test: $\chi^2 = 8.5$, $p = 0.004$. (**G**) Mean (black bars) and individual (circles) thresholds of Aβ SA-LTMRs in control (left, $n = 11$ cells) and *TrkB*^{cKO} mice (right, $n = 15$ cells). Unpaired Student's *t* test: $t = -0.81$, $p = 0.42$.

behavior: forepaw manipulation of sunflower seeds while eating. The amount of time required to deshell and eat the sunflower seed kernel was comparable for control and *TrkB*^{cKO} mice. However, whereas control mice used their forepaws to hold, elevate, and rotate the sunflower seed, *TrkB*^{cKO} mice typically trapped or braced the seed on the floor while biting and removing the shell to expose the kernel (Fig. 2G and movies S1 and S2). *TrkB*^{cKO} mice exhibited fewer forepaw dips to the floor and seed rotations and instead more frequently touched the floor to brace the seed (Fig. 2G). By contrast, gait was largely unaltered in *TrkB*^{cKO} mice, although subtle differences in gait were apparent at high velocities (fig. S4). We observed no other obvious sensorimotor deficits in *TrkB*^{cKO} mice (figs. S3 and S4).

Meissner corpuscles are dually innervated

Large-diameter, myelinated sensory neurons innervating Meissner corpuscles express the tyrosine kinase Ret beginning on embryonic day 10.5 (E10.5) (*9*). Consistent with this, *Ret*^{CreER}; *Rosa26*$^{LSL\text{-}tdTomato}$ mice (*9*, *17*) treated with tamoxifen from E10.5 to E13.5 had tdTomato$^+$ sensory fibers that innervate Meissner corpuscles (Fig. 3A). Because TrkB$^+$ sensory neurons are required for Meissner corpuscle formation, we asked whether these Ret$^+$ Meissner afferent fibers also express TrkB. TrkB$^+$ axon terminals were present in the dermal papillae of glabrous skin during embryonic and early postnatal ages, but TrkB expression was undetectable in Meissner afferent terminals in adult mice (fig. S5). Therefore, to permanently label TrkB$^+$ neurons and visualize their cutaneous endings in glabrous skin of adults, we treated *TrkB*^{CreER}; *Rosa26*$^{LSL\text{-}tdTomato}$ mice (*18*) with tamoxifen between E15.5 and P6. We observed that adult *TrkB*^{CreER}; *Rosa26*$^{LSL\text{-}tdTomato}$ mice possess tdTomato$^+$ sensory fibers within Meissner corpuscles (Fig. 3B). These TrkB$^+$ Meissner corpuscle afferents are distinct from Ret$^+$ Meissner corpuscle afferents. Indeed, using *TrkB*^{CreER}; *Rosa26*$^{LSL\text{-}tdTomato}$; *Ret*^{CFP} compound mice (*19*), the TrkB$^+$ and Ret$^+$ sensory neurons were found to be separate populations, with endings of both of these neuronal populations terminating within the majority of corpuscles in both forepaw and hindpaw glabrous skin (Fig. 3, C and E). Dual innervation of corpuscles was also seen using the *Npy2r-GFP* BAC transgenic mouse line, which labels Aβ RA-LTMRs in both hairy and glabrous skin (*20*) (GFP, green fluorescent protein). In *TrkB*^{CreER}; *Rosa26*$^{LSL\text{-}tdTomato}$; *Npy2r-GFP* compound mice, all GFP$^+$ fibers in the dermal papillae were tdTomato$^+$ (fig. S5). On the other hand, in *Ret*^{CreER}; *Rosa26*$^{LSL\text{-}tdTomato}$; *Npy2r-GFP* compound mice, tdTomato$^+$ and GFP$^+$ fibers in dermal papillae were distinct and intertwined (Fig. 3D). Both the Ret$^+$ and TrkB$^+$ Meissner afferents expressed neurofilament, and together

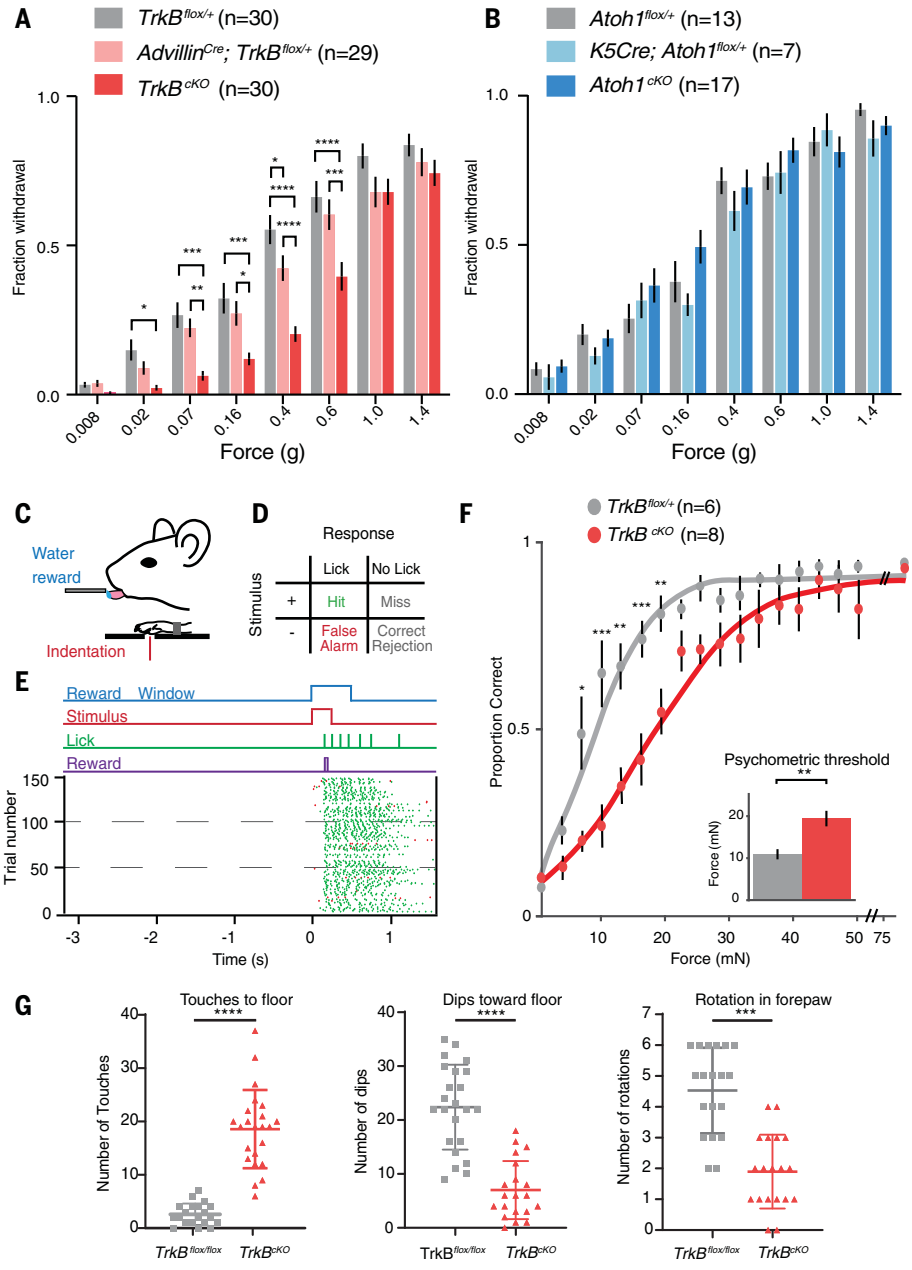

Fig. 2. Meissner corpuscles are necessary for light touch perception and fine sensorimotor control. (**A**) Fraction (mean ± SEM) of paw withdrawals to von Frey filament applications for *TrkB*^{cKO} and control mice. Repeated measures (RM) two-way analysis of variance (ANOVA), effect of genotype ($F_{2,86}$ = 9.823, p = 0.0001) with post hoc Tukey's test; p values represent comparisons between genotypes for each filament: *p < 0.05, **p < 0.01, ***p < 0.001, and ****p < 0.0001. (**B**) Same as (A) for *Atoh1*^{cKO} and control mice. RM two-way ANOVA, no effect of genotype: $F_{2,34}$ = 0.8258, p = 0.4465. (**C**) Operant conditioning task design. (**D**) Matrix of possible behavioral outcomes from one trial. (**E**) Operant conditioning task. The stimulus paradigm, in which animals must withhold for at least 3 s before initiation of a new trial, is depicted (top). In trials with a stimulus (shown), animals receive rewards only on hit trials. Raster plot of licks is shown (bottom). Hit trials are shown with green ticks; false alarm trials are shown with red ticks. (**F**) Psychometric functions for the operant conditioning task for *TrkB*^{cKO} and control mice. Error bars represent SEM (the inset shows thresholds; unpaired Student's t test: t = 2.69, p = 0.002). Two-way ANOVA, effect of genotype ($F_{1,12}$ = 8.261, p = 0.0140) with post hoc Sidak's multiple comparison text; p values represent comparisons between genotypes for each force range: *p < 0.05, **p < 0.01, and ***p < 0.001. (**G**) The number of sunflower seed touch-taps when the seed is braced against the floor between forepaws during seed peeling is shown on the left. The number of times the mouse held the seed in an elevated position and used its incisors to bite into the seed while applying downward force (dips) to expose seed kernel is shown in the middle. The number of seed rotations as mice adjusted their grasp is shown on the right. Unpaired Student's t test, ***p < 0.001 and ****p < 0.0001.

these two neuronal populations accounted for most, if not all, NFH$^+$ Meissner corpuscle endings (Fig. 3C and fig. S5). Meissner corpuscle lamellar cells, which are specialized terminal Schwann cells, migrated into dermal papillae along Meissner afferent axons during development (fig. S6), and TrkB$^+$ axons and corpuscle lamellar cells were both absent from dermal papillae of *TrkB*^{cKO} mice. Although axons of Ret$^+$ neurons still projected into dermal papillae in the absence of TrkB$^+$ axons and corpuscle lamellar cells in neonatal *TrkB*^{cKO} mutants, these Ret$^+$ fibers either retracted or degenerated because neither Ret$^+$ nor TrkB$^+$ afferents were present in dermal papillae of adult *TrkB*^{cKO} mice (fig. S2). Thus, consistent with prior work suggesting multiple, immunohistochemically distinct Meissner corpuscle afferent endings (*21*), our findings reveal that Meissner corpuscles are co-innervated by a pair of intertwined, molecularly and developmentally distinct populations of sensory neurons, one expressing TrkB and another expressing Ret.

Meissner afferents exhibit distinct response properties

Meissner corpuscles are believed to be innervated by one physiological type of sensory neuron, the Aβ RAI-LTMR (*21*–*24*). Our electrophysiological recordings showed that Aβ RA-LTMR responses to glabrous skin stimulation are lost in *TrkB*^{cKO} mice (Fig. 1F). Therefore, we hypothesized that the Ret$^+$ and TrkB$^+$ Meissner afferents are previously unrecognized subsets of Aβ RAI-LTMRs. Aβ RA-LTMRs form central collaterals along the rostrocaudal axis of the spinal cord and also extend an axonal branch via the dorsal column to the dorsal column nuclei (DCN) of the brainstem (*25*–*27*). This projection via the direct dorsal column pathway is likely important for tactile perception and discriminative touch (*21*). We visualized the central projections of both the Ret$^+$ and TrkB$^+$ Meissner afferents. These analyses revealed that both Meissner afferent subtypes display archetypal Aβ LTMR central collateral morphologies and axonal projections to the DCN (fig. S7).

We next asked whether either or both Ret$^+$ and TrkB$^+$ Meissner afferents have physiological response properties consistent with those of Aβ RAI-LTMRs. We used the in vivo DRG recording preparation for targeted electrophysiological recordings of genetically labeled Ret$^+$ and TrkB$^+$ Meissner afferent populations. All recorded Meissner afferents of both subtypes had small, well-defined receptive fields confined to a single glabrous pad. Both subtypes also had conduction velocities within the Aβ range, although the mean conduction velocity of TrkB$^+$ Meissner afferents was modestly but significantly slower than that of Ret$^+$ Meissner afferents (Fig. 4A). TrkB$^+$ Meissner

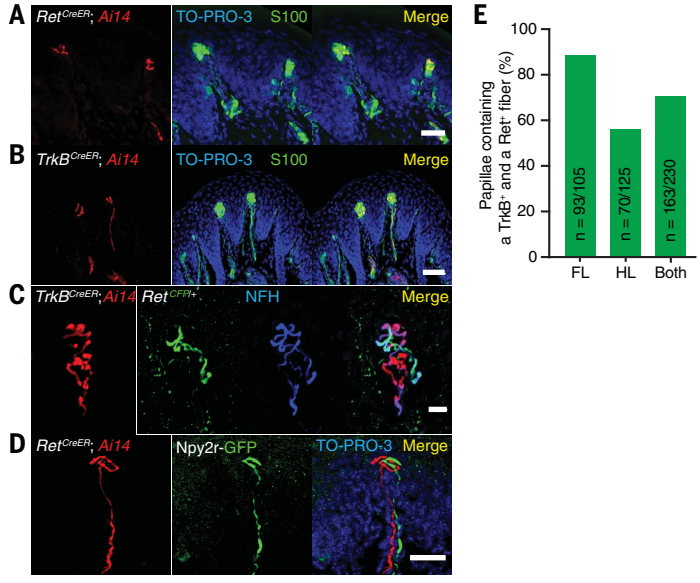

Fig. 3. Meissner corpuscles are innervated by two molecularly distinct mechanosensory neuron types. (**A**) Forelimb pedal pad section of a P20 *Ret*^{CreER}; *Rosa26*$^{LSL\text{-}tdTomato}$ (*Ai14*) mouse treated with tamoxifen at E10.5 to E11.5. The section is stained for S100, DsRed, and TO-PRO-3. This experiment was repeated in three mice. Scale bar, 25 μm. (**B**) Hindlimb digital pad section of a P50 *TrkB*^{CreER}; *Rosa26*$^{LSL\text{-}tdTomato}$ (*Ai14*) mouse treated with tamoxifen at E16.5. The section is stained for S100, DsRed, and TO-PRO-3. This experiment was performed in eight mice with varying dates of tamoxifen administration (E13.5, E16.5, P2, and P6). Scale bar, 50 μm. (**C**) Hindlimb digital pad section of a P50 *TrkB*^{CreER}; *Ai14*; *Ret*^{CFP} mouse treated with tamoxifen at P5. The section is stained for DsRed, GFP, and NFH. This experiment was repeated in four mice with tamoxifen administration at E13.5 or P5. Scale bar, 10 μm. (**D**) Forelimb pedal pad section of a P20 *Ret*^{CreER}; *Ai14*; *Npy2r-GFP* mouse treated with tamoxifen at E10.5. The section is stained with anti-DsRed, anti-GFP, and TO-PRO-3. This experiment was repeated in three mice. Scale bar, 25 μm. (**E**) Percentage of dermal papillae containing both TrkB$^+$ and Ret$^+$ Meissner afferents in forelimb pads, hindlimb pads, and all pads, as measured in *TrkB*^{CreER}; *Ai14*; *Ret*^{CFP} mice (two animals). Only papillae containing a tdTomato$^+$ fiber were included in the quantification to eliminate an effect of Cre-lox efficiency on the interpretation of these measurements.

afferents responded at both the onset and offset of force-controlled step indentations with high sensitivity, whereas Ret$^+$ Meissner afferents responded at the onset of step indentations with lower and more varied sensitivity and rarely responded to the offset of step indentations (Fig. 4, B to D). Some (4 of 10) of the Ret$^+$ Meissner afferents responded during the sustained phase of the step indentation (example in Fig. 4E), indicating that Meissner-innervating afferents are not always rapidly adapting. Both TrkB$^+$ and Ret$^+$ Meissner afferents exhibited a wide range of frequency tuning to 2- to 120-Hz sinusoidal vibrations: Some neurons of both types responded best to high frequencies, whereas others had nearly uniform force thresholds across the tested frequencies (fig. S8). Although frequency tuning did not differ between TrkB$^+$ and Ret$^+$ Meissner afferents, TrkB$^+$ Meissner afferents were more sensitive to vibratory stimuli than Ret$^+$ Meissner afferents (fig. S8). Altogether, although the response properties of TrkB$^+$ Meissner afferents fit the classic Aβ RAI-LTMR definition, those of most Ret$^+$ Meissner afferents do not.

Ret$^+$ and TrkB$^+$ Meissner afferents are homotypically tiled and heterotypically offset

We next investigated the spatial relationships between the cutaneous termination fields of Ret$^+$ and TrkB$^+$ Meissner afferents. Homotypic tiling is a phenomenon in which the anatomical receptive fields of neurons do not spatially overlap with other neurons of their same type. Using whole-mount alkaline phosphatase (AP) staining of sparsely labeled Meissner afferents, we found that the skin innervation areas of individual Ret$^+$ and TrkB$^+$ Meissner afferents are well demarcated, spatially contiguous, and confined to single glabrous pads (fig. S9), consistent with the physiological receptive fields being confined to single glabrous pads. Occasionally, two neurons innervating the same toe or pedal pad were labeled (Fig. 5A). In these cases, TrkB$^+$ afferents were never observed to spatially overlap, and only 1 out of 10 pairs of Ret$^+$ afferents occupying the same pad displayed spatial overlap (Fig. 5C). For the single overlapped Ret$^+$ afferent pair, the two arborizations shared only 1 out of 12 total corpuscles, and this corpuscle was on the border of their termination fields. We also used an intersectional genetic labeling strategy to address homotypic tiling. We generated mice harboring either the *TrkB*^{CreER} or *Ret*^{CreER} allele in conjunction with two different Cre-dependent fluorescent reporters, *Rosa26*$^{LSL\text{-}YFP}$ and *Rosa26*$^{LSL\text{-}tdTomato}$. We treated these mice with high doses of tamoxifen to randomly and efficiently label individual afferents with one of three possibilities: tdTomato, yellow fluorescent protein (YFP), or both. Virtually all Meissner corpuscles examined in these mice contained a single-color fiber of a given afferent subtype (Fig. 5, B and D), thus confirming homotypic tiling of the two Meissner afferent types. We also compared the peripheral arborizations of sparsely labeled Ret$^+$ and TrkB$^+$ Meissner corpuscle afferents. These two populations exhibited differences in both their surface-area size distributions and the number of Meissner corpuscles innervated by individual neurons (Fig. 5, E and F, and fig. S9), indicating that the two homotypically tiled Meissner afferent types are heterotypically offset.

One potential advantage of heterotypic overlap of Meissner mechanoreceptors with different force sensitivities is to enable discrimination of a greater range of forces. In this model, spikes emanating from the TrkB$^+$ Meissner Aβ LTMR alone encode the lightest indentation forces, whereas spikes from both TrkB$^+$ and Ret$^+$ Meissner mechanoreceptors encode higher forces. Another potential advantage of heterotypic overlap of homotypically tiled Meissner mechanoreceptors is that population responses to forces that coactivate both Meissner afferent types could enable a heightened ability to detect and localize a point stimulus. We modeled the receptive fields of each of the two Meissner afferent subtypes as homotypically tiled grids that are heterotypically offset and simulated measurements of spatial acuity (fig. S10). Our simulations indicated that for a single nonoverlapping grid, the number of discriminable spatial locations is equal to the number of neurons (fig. S10). Simulations using two grids that are homotypically tiled but overlapping and maximally offset with respect to each other revealed that the number of distinct spatial locations doubles for the same number of neurons (fig. S10). This gain arose from a distributed neural representation that an overlapped arrangement facilitates and may enable an enhanced ability to localize a point stimulus without increasing the number of neurons. Therefore, although functional analyses of mice selectively lacking one or the other Meissner afferent subtype will be needed to test our mathematical modeling findings, we speculate that the heterotypic overlap of homotypically tiled Meissner mechanoreceptor subtypes may enable heightened discriminatory capabilities, at a population level, compared with a simpler arrangement of a single homotypically tiled Meissner afferent type.

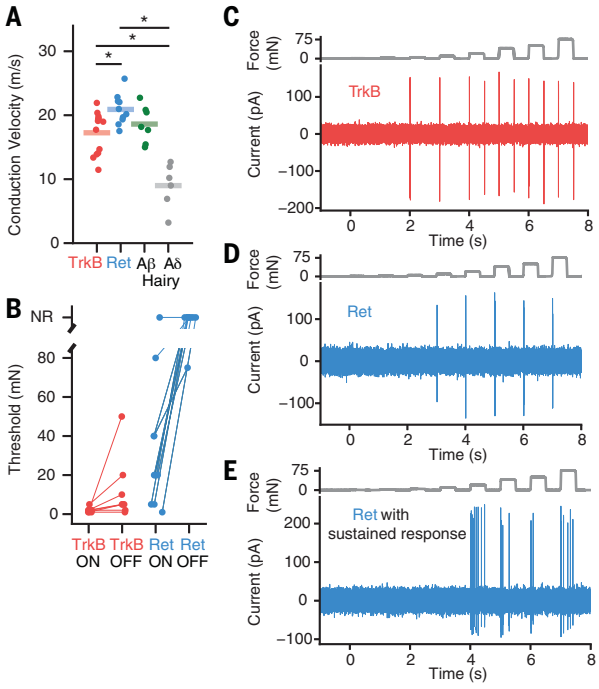

Fig. 4. Ret$^+$ and TrkB$^+$ Meissner afferents exhibit distinct physiological response properties. (**A**) Both Meissner afferent subtypes have conduction velocities in the Aβ range as defined by the range of conduction velocities measured from hairy skin Aδ and Aβ LTMRs in the same preparation. The average conduction velocities for TrkB$^+$ and Ret$^+$ Meissner afferents are significantly different [10 afferents per type; mean ± SEM: TrkB = 17.3 ± 0.9 m/s and Ret = 20.9 ± 0.8 m/s; Mann-Whitney *U* test (U = 26.0, p = 0.008)]. *p < 0.05. (**B**) The minimal force required to produce an action potential at the onset or offset of a step indentation for TrkB$^+$ and Ret$^+$ Meissner afferents. NR, not responsive. (**C**) Response of a TrkB$^+$ Meissner Aβ LTMR to a series of step indentations increasing in intensity from 1 to 75 mN. (**D**) Response of a RA Ret$^+$ Meissner afferent to the same stimuli as in (C). (**E**) Response of a SA Ret$^+$ Meissner afferent to the same stimuli as in (C).

Ret$^+$ and TrkB$^+$ Meissner afferents have distinct lamellar cell associations

The different sensitivities and response kinetics of Ret$^+$ and TrkB$^+$ Meissner Aβ mechanoreceptors raised the question of whether these mechanoreceptor types form distinct endings within the corpuscle where mechanotransduction occurs. We evaluated the ultrastructural properties of the axonal endings of Ret$^+$ and TrkB$^+$ Aβ mechanoreceptors within the Meissner corpuscle using electron microscopy (EM). We crossed *Ret*^{CreER} or *TrkB*^{CreER} mice to reporter mice that express the peroxidase dAPEX2 targeted to the mitochondrial matrix in a recombinase-dependent manner (*28*), thereby generating an electron-dense label associated with mitochondria and distributed throughout the labeled cells. We could distinguish and characterize the ultrastructural properties of labeled Aβ mechanoreceptors within the Meissner corpuscle. Axons of both Ret$^+$ and TrkB$^+$ mechanoreceptor subtypes terminated within the Meissner corpuscle, and both ending types were intimately associated with resident, morphologically complex corpuscle lamellar cells (Fig. 6, A and B). The lamellar cell processes that surround both Meissner mechanoreceptor ending types were periodically discontinuous, thus exposing the naked mechanoreceptor axonal membrane to the extracellular matrix (Fig. 6C). Whereas Ret$^+$ Meissner axon profiles were usually surrounded by only a few concentrically arranged lamellar cell processes, the lamellar cell processes associated with TrkB$^+$ Meissner profiles were typically much more elaborate. Indeed, TrkB$^+$ Meissner afferents have a minimum of five concentric lamellar processes surrounding the axon terminal (range 5 to 28) and, on average, twice as many processes compared with Ret$^+$ Meissner afferent terminals (range 3 to 18; Fig. 6D). This ultrastructural difference is particularly noteworthy when considering the distinct response kinetics of Ret$^+$ and TrkB$^+$ Meissner afferents together with classical studies of the Pacinian corpuscle suggesting that lamellar wrappings are critical for the Pacinian LTMR's response kinetics (*29*). For the Pacinian afferent, lamellar cell wrappings are believed to be essential for its high selectivity to vibratory stimuli and for producing a generator potential as force is withdrawn during a step offset. Moreover, "unwrapping" or removing Pacinian lamellar cells converted its generator potential from being transient to sustained (*29*). Our findings that Ret$^+$ Meissner mechanoreceptors are associated with fewer lamellar cell wrappings compared with the TrkB$^+$ Meissner LTMR and that they lack responses at indentation step offsets and occasionally display slowly adapting responses are consistent with these classical theories.

Conclusions

Our findings show the Meissner corpuscle to be crucial for perception of the gentlest detectable forces acting on the glabrous skin and for fine sensorimotor control during object manipulation. The corpuscle is endowed with intertwined endings of two molecularly, ultrastructurally, and physiologically distinct mechanoreceptor subtypes whose cutaneous innervation areas are homotypically tiled and heterotypically offset. This arrangement of differentially sensitive Meissner Aβ mechanoreceptors supports a "population coding" model for force intensity. Computational simulations suggest that it may enable higher acuity, at a population level, than would be expected from a simpler arrangement with a single Meissner mechanoreceptor subtype. The organization of the Meissner corpuscle afferents' termination fields thus illustrates a solution to the nervous system's general challenge of localizing stimuli with a limited number of neurons. Our EM findings reveal that the axonal endings of the Ret$^+$ and TrkB$^+$ Meissner Aβ mechanoreceptor subtypes, and in particular their association with concentrically organized processes of corpuscle lamellar cells, are distinct, supporting a model in which ultrastructural properties of mechanoreceptors within a corpuscle dictate their responses.

Materials and methods

Animals

Animals were handled according to protocols approved by the Harvard Standing Committee on Animal Care and are in accordance with federal guidelines.

Mouse lines

The *TrkB*^{flox}, *Advillin*^{Cre} (JAX 032536), *K5Cre* (MGI 3050065), *Atoh1*^{flox} (JAX 008681), *Ret*^{CreER} (MGI #4437245), *Ai14* (*Rosa26*$^{LSL\text{-}tdTomato}$; JAX 007914), *Ret*^{CFP} (MGI 3777555), *Npy2r-GFP* (MGI 3844094), *Rosa26*^{iAP} (JAX 009253), *Ai3* (*Rosa26*$^{LSL\text{-}YFP}$; JAX 007903), *Ai32* (*Rosa26*$^{LSL\text{-}ChR2(H134R)\text{-}EYFP}$; JAX 024109), *TrkB*^{CreER} (JAX 027214), *Pvalb*$^{2A\text{-}FlpO\text{-}D}$ (JAX 022730), *Ai65* (*Rosa26*$^{FSF\text{-}LSL\text{-}tdTomato}$; JAX 021875), *Rosa26*$^{LSL\text{-}FSF\text{-}ReaChR\text{-}mCitrine}$ (JAX 024846), *Rosa26*$^{DR\text{-}Matrix\text{-}dAPEX2}$ (JAX 032764), *Rosa26*$^{LSL\text{-}Matrix\text{-}dAPEX2}$ (JAX 032765), *Brn3a*$^{f(AP)}$ (JAX 010558), *BDNF*^{lacZ} (*BDNF*^{flox}; JAX 021055), *Wnt1Cre* (JAX 022137), and *DhhCre* (JAX 012929) mouse lines have been described previously (*5*, *6*, *9*, *14*, *15*, *17*–*20*, *28*, *30*–*38*). The *Advillin*^{FlpO} mouse line, which was generated by standard gene targeting procedures, enables FlpO-dependent recombination in somatosensory and other peripheral nervous system neurons and will be described in detail elsewhere. All lines were kept on a mixed CD1-C57Bl/6 background.

Tamoxifen treatments

Tamoxifen (Toronto Research Chemicals) was dissolved in 100% ethanol (20 mg/ml). The tamoxifen-ethanol mixture was diluted with sunflower seed oil (Sigma) at a 1:2 to 1:3 dilution and vacuum centrifuged for 30 to 45 min until the ethanol evaporated. The resulting solution was stored at −20°C and thawed immediately before use. For embryonic tamoxifen treatment, the oil-tamoxifen solution was delivered to pregnant mothers by oral gavage. The

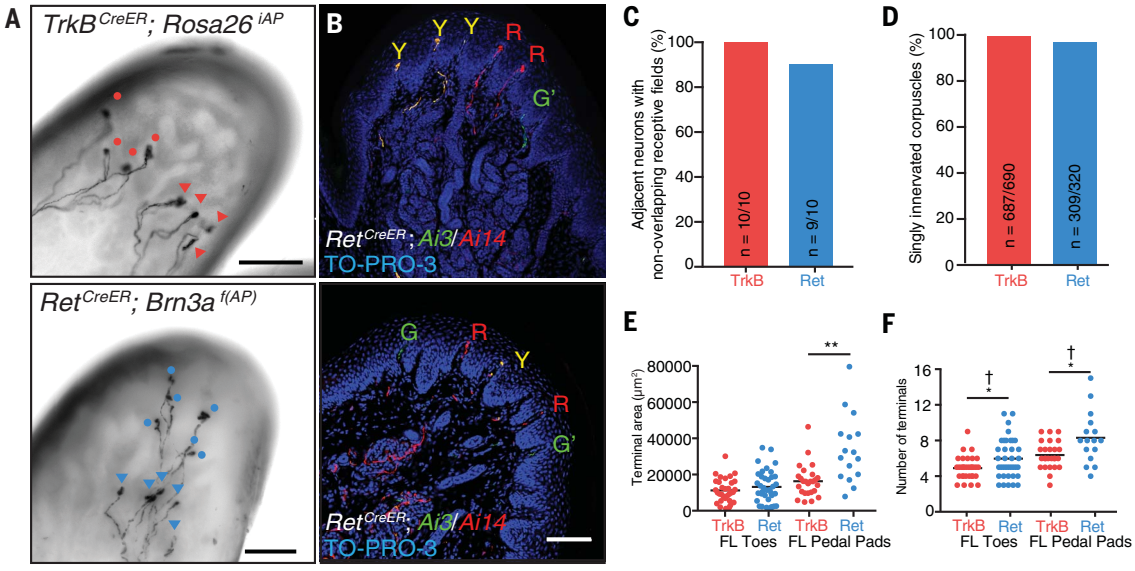

Fig. 5. Spatial arrangement of Ret$^+$ and TrkB$^+$ Meissner afferent cutaneous endings. (**A**) Images of whole-mount, AP-stained digital pads of a *TrkB*^{CreER}; *Rosa26*^{iAP} mouse (top) and a *Ret*^{CreER}; *Brn3a*$^{f(AP)}$ mouse (bottom, Z-projection performed in Fiji), depicting pairs of afferents of the same subtype innervating the same glabrous pad. Tamoxifen doses were titrated to achieve sparse labeling of Meissner afferents. Terminals of one neuron are annotated with circles and terminals of the other with triangles. Scale bars, 100 μm. (**B**) Digital pad sections of *TrkB*^{CreER}; *Rosa26*$^{LSL\text{-}YFP/LSL\text{-}tdTomato}$ (*Ai3/Ai14*) mice treated with tamoxifen at E12.5 and E13.5 (top) and *Ret*^{CreER}; *Ai3/Ai14* mice administered tamoxifen at E11.5 and E12.5 (bottom). Y, fibers express both tdTomato and YFP; R, fibers express tdTomato only; G, fibers express YFP only; G', YFP$^+$ fibers without terminals in the sections. Sections were stained with anti-DsRed, anti-GFP, and TO-PRO-3. Scale bar, 100 μm. (**C**) Percentage of TrkB$^+$ and Ret$^+$ Meissner afferent pairs innervating the same pad and occupying different spatial territories. (**D**) Quantification of the percentage of dermal papillae and Meissner corpuscles receiving a single TrkB$^+$ fiber (three animals) and a single Ret$^+$ fiber (six animals). (**E** and **F**) Receptive field surface area [terminal area, (E)] and number of terminal endings (F) of TrkB$^+$ and Ret$^+$ Meissner afferents measured in *TrkB*^{CreER}; *Rosa26*^{iAP} or *TrkB*^{CreER}; *Brn3a*$^{f(AP)}$ mice [58 forelimb (FL) receptive fields from 21 mice] and *Ret*^{CreER}; *Rosa26*^{iAP} or *Ret*^{CreER}; *Brn3a*$^{f(AP)}$ mice (53 FL receptive fields from 21 mice). Individual measurements and mean values (black bar) are plotted for forelimb digital pads and pedal pads (two-tailed Welch's *t* test, mean significantly different: $*p < 0.05$ and $**p < 0.01$; *F* test of the equality of variances, variance significantly different: $\dagger p < 0.01$).

Ret$^+$ Meissner afferent population was labeled with high efficiency by giving pregnant mothers a 2-mg dose of tamoxifen at E11.5 and E12.5. The forelimb was labeled more effectively at E11.5, whereas the hindlimb was labeled more effectively at E12.5. The TrkB$^+$ Meissner afferent population was labeled with high efficiency by intraperitoneal injection at P4, but this population was also labeled when pregnant mothers were given tamoxifen any time between E12.5 and E16.5 (2 mg) and when P2 to P6 pups were given tamoxifen (0.04 to 0.1 mg/g body weight).

Immunohistochemistry

P20 or older mice were euthanized with CO_2 and perfused with Ames Media (Sigma) containing 10 U/ml heparin (Sigma) in phosphate-buffered saline (PBS), followed by 4% paraformaldehyde (PFA) in PBS. Spinal cords and brainstems were dissected and fixed in 4% PFA at 4°C overnight. For skin sectioning experiments, glabrous toe and pedal pads were removed from the paw and placed in 4% PFA for 4 to 6 hours or Zamboni's fixation buffer for 24 to 48 hours at 4°C. For whole-mount immunohistochemistry, whole paws were placed in Zamboni's fixation buffer at 4°C for 24 to 48 hours. The glabrous skin was then separated from the underlying tissue by fine dissection in PBS. Isolated glabrous paws were fixed in Zamboni's fixation buffer for an additional 1 hour at room temperature. Following fixation, all tissues were rinsed three times for 10 min in PBS at room temperature. Brainstems and spinal cords with dorsal root ganglia attached were isolated from the vertebral column.

Glabrous pads, spinal cords, and brainstems destined for sectioning were cryoprotected in 30% sucrose in PBS at 4°C for 24 to 48 hours. Tissues were embedded in optimal cutting temperature (OCT) compound (Tissue Tek) and frozen at −20°C. Glabrous pads were sectioned at 25 μm, and spinal cords and brainstems were sectioned transversely at 40 to 50 μm. Sections were dried overnight at room temperature. Glabrous pads were given one to two additional days to dry. All sections were rinsed three times for 10 min with PBS, blocked with 5% normal serum (donkey or goat) in 0.1% PBST (0.1% Triton X-100 in PBS) for 2 hours, and incubated with primary antibody in blocking solution overnight at 4°C. The following day, sections were rinsed three times for 10 min with PBST and incubated with secondary antibodies in blocking solution for 2 hours at room temperature or overnight at 4°C. Sections were then rinsed once for 10 min in PBST and twice for 10 min in PBS and mounted with Fluoromount-G (Southern Biotech). Images were acquired on a Carl Zeiss LSM 700 confocal microscope.

Whole-mount immunohistochemistry of glabrous skin was performed as described previously (7). The skin was given several 1-hour washes in 0.3 to 0.5% TritonX-100 in PBS. The skin was then incubated in primary antibodies in blocking solution [5% normal serum (goat or donkey), 75% PBST, 20% DMSO] at room temperature for 72 hours. The skin was washed in PBST for four to five times for 1 hour and incubated in secondary antibodies in blocking solution at room temperature for 48 hours. Tissue was washed several times in PBST then dehydrated in serial methanol dilutions (1 hour each of 25%, 50%, 75%, and 100%), followed by overnight dehydration in 100% methanol at room temperature. The tissue was then cleared in BABB (1 part benzyl alcohol: 2 parts benzyl benzoate) and imaged.

Primary antibodies were rabbit anti-DsRed (Clontech, cat. no. 632496, 1:500), goat anti-mCherry (Sicgen, cat. no. AB0040-200, 1:500), chicken anti-GFP (Aves Lab, cat. no. GFP-1020, 1:500), rabbit anti-GFP (Invitrogen, cat. no. A-11122, 1:500), goat anti-GFP (US Biological, cat. no. G8965-01E, 1:500), rat anti-MBP (Millipore, cat. no. MAB386, 1:500), rabbit anti-NFH (Sigma, cat. no. N4142, 1:1000), chicken anti-NFH (Aves Lab, cat. no. NFH, 1:500), rabbit anti-S100 (Dako, cat. no. Z031129-2, 1:300), rabbit anti-PKC γ (Santa Cruz, cat. no. SC-211, 1:500), and TROMA-I (rat anti-keratin 8/cytokeratin 18, DSHB, University of Iowa, TROMA-I supernatant, 1:100). The nucleic acid stain TO-PRO-3 (Invitrogen, cat. no. T3605, 1:500), the nonpeptidgeric nociceptor

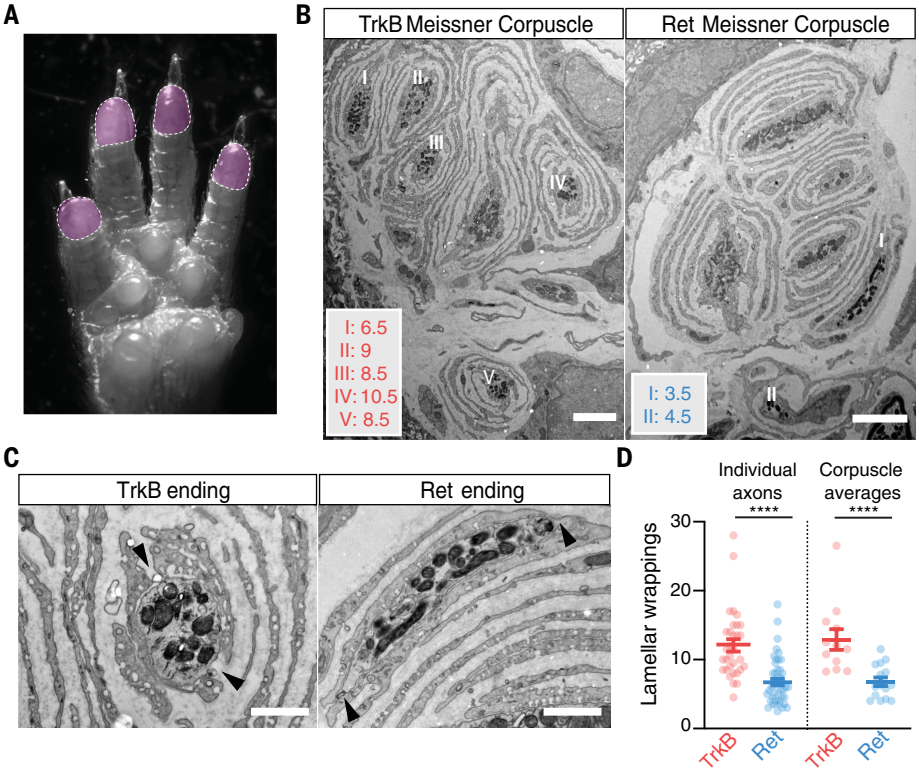

Fig. 6. TrkB$^+$ Meissner Aβ LTMR endings have more lamellar cell wrappings than Ret$^+$ Meissner mechanoreceptor endings. (**A**) Image of a paw, with the shaded areas (digit tips) representing regions used for EM analysis that contain a high density of Meissner corpuscles. (**B**) EM images of Meissner corpuscles from a *TrkB*^{CreER}; *Advillin*^{FlpO}; *Rosa26*$^{DR\text{-}Matrix\text{-}dAPEX2}$ mouse treated with tamoxifen at P3 (left) and a *Ret*^{CreER}; *Advillin*^{FlpO}; *Rosa26*$^{DR\text{-}Matrix\text{-}dAPEX2}$ mouse treated with tamoxifen at E11.5 and P10 (right). Roman numerals mark labeled TrkB (left) and Ret (right) axons. The number of lamellar wrappings for individual labeled axonal profiles is shown. Scale bars, 3 μm. (**C**) High-magnification images of labeled endings and associated lamellar cells from (B). Both exhibit openings or areas not directly associated with lamellar cells (black arrowheads). Scale bars, 1 μm. (**D**) Quantification of the number of lamellar cell wrappings around genetically labeled endings of TrkB and Ret endings. Shown are the number of lamellar wrappings for individual axonal profiles (left; n = 32 and 47, respectively) and averages of all axonal profiles within individual corpuscles (right; n = 12 and 15, respectively). Mann-Whitney U test, ****$p < 0.0001$. Corpuscles imaged from two mice for each LTMR subtype.

marker IB4 (Isolectin GS-IB$_4$, conjugated to Alexa Fluor 647, Life Technologies, cat. no. I32450, 1:500), and the nucleic acid stain Hoechst 33258 (Fisher, cat. no. H3569, 1:1000) were applied during secondary antibody incubation.

X-gal staining

Embryos and glabrous skin were fixed with a glutaraldehyde solution (0.2% glutaraldehyde, 2 mM $MgCl_2$ in PBS) overnight at 4°C. For whole-mount staining, fixed embryos or skin were washed with detergent rinse buffer (0.01% sodium deoxycholate, 0.02% NP40, 2 mM $MgCl_2$ in phosphate buffer, pH 7.4) and stained with staining buffer (0.01% sodium deoxycholate, 0.02% NP40, 2 mM $MgCl_2$, 5mM potassium ferricyanide, 5mM potassium ferrocyanide, 1mg/ml 5-bromo-4-chloro-indolyl-β-D-galactopyranoside in phosphate buffer, pH 7.4) at room temperature. After staining, embryos were dehydrated sequentially with 50% methanol, 80% methanol, and 100% methanol. For staining on sections, 12-μm sections were cut and dried for several hours at room temperature. The staining procedure was the same as described for whole-mount staining. After staining, sections were fixed overnight at 4°C in 4% PFA in PBS, and mounted with Fluoromount-G.

Fluorescent sparse labeling

TrkB$^+$ Meissner afferents were sparsely labeled by injecting the pedal pads of *TrkB*^{CreER}; *Ai65* mice with a viral vector containing FlpO recombinase, AAV1-hSyn-FlpO (AAV2/1.humanSynapsin1.FlpO.bGH, UPenn Vector Core, titer = 1.23×10^{13} genome copies/ml). Mice were administered 0.5 mg of tamoxifen at P5 by interperitoneal injection. Mice aged P9 were anesthetized with isoflurane (2 to 3%) delivered from a precision vaporizer. Animals were monitored throughout the 5- to 10-min procedure, and the anesthetic dose was adjusted as necessary. AAV1-hSyn-FlpO combined with a small amount of Fast Green dye (Sigma F7252-5G) in 0.9% saline was injected into one to three hindlimb or forelimb pedal pads per animal with a beveled glass capillary needle (FHC Inc capillary tubing, FHC 27-30-0). The total volume of AAV–Fast Green mixture injected per pad for sparse labeling was about 0.1 to 0.5 μl. Mice were removed from anesthesia, administered analgesic (Carprofen, 4 mg/kg), and placed on a warm pad for recovery. Animals were given an additional dose of Carprofen after 24 hours and observed to ensure adequate recovery. Mice were perfused 2 to 9 weeks after injection, and their vertebral columns and glabrous paws were prepared as described above. The viral dose was titrated to achieve labeling of a single neuron per animal, and only mice in which a single cervical or lumbar neuron was observed in the DRG were included in subsequent analyses.

Alkaline phosphatase histochemistry

Placental alkaline phosphatase (PLAP) staining was performed as described previously (*6*). Whole paws from P21 mice were fixed in Zamboni's fixation buffer at 4°C for 24 to 48 hours. Age was kept consistent to prevent age and size differences from contributing to observed differences between Ret$^+$ Meissner afferent and TrkB$^+$ Meissner afferent receptive fields. The glabrous skin was then separated from the underlying tissue by fine dissection in PBS. Isolated glabrous paws were fixed in Zamboni's fixation buffer for an additional 1 hour at room temperature. After fixation, all tissues were rinsed three times for 10 min in PBS at room temperature and then incubated at 65° to 68°C for 2 hours. To detect PLAP signal, tissues were incubated with BCIP/NBT (Roche) solution (diluted in 0.1 M Tris pH 9.5, 0.1 M NaCl, 50 mM $MgCl_2$, 0.1% Tween-20 solution) overnight at room temperature. Tissues were then fixed in 4% PFA in PBS for 1 hour at room temperature, followed by dehydration in ethanol (1 hour 50%, 1 hour 75%, 1 hour 100%, overnight 100%). Finally, tissues were cleared in BABB and imaged.

To sparsely label Ret$^+$ Meissner afferents, pregnant mice were administered 1 mg tamoxifen at either E11.5 or E12.5. For TrkB$^+$ Meissner afferents, pregnant mice were administered 1 mg tamoxifen at E14.5.

Quantification of receptive field geometries

Images of Meissner afferent terminal arborizations in glabrous pads were analyzed in the Fiji distribution of ImageJ (www.fiji.sc). The perimeter of individual receptive fields (terminal area) was outlined by hand, and the resulting selection was subjected to the Convex Hull function, which replaces a polygon with its convex hull. The area in μm^2 and the aspect ratio (major axis/minor axis) of the convex hull were measured using the measure function. Terminals of afferent arborizations were counted by eye. For some neurons, two fibers from the

same neuron could be seen traveling together and terminating in the same corpuscle. In these cases, the two fibers were counted as a single termination. This phenomenon appeared to occur more often for $TrkB^+$ Meissner afferents than for Ret^+ Meissner afferents, but this was not quantified.

In vivo electrophysiological recordings

In vivo DRG recordings were made as described previously (*7*) using a preparation modified from that published by Ma, Donnelly, and LaMotte (*8*). Ret^{CreER} or $TrkB^{CreER}$ mice with a Cre-dependent YFP, tdTomato, or mCitrine reporter (*Ai14*, *Ai32*, or $Rosa26^{LSL\text{-}ReaChR\text{-}mCitrine}$) were administered tamoxifen at the appropriate ages. Because this strategy also labels hairy-skin-innervating neurons, we retrogradely labeled glabrous neurons by subcutaneous injection of cholera toxin subunit B conjugated to Alexa 555 or Alexa 488 (Thermo Fisher; 2 μg/μl in PBS, about 0.3 μl per pad) into the left hindlimb toe and pedal pads 2 to 3 days before recording. On the day of recording, P20 to P60 mice were anesthetized with urethane (1 g/kg) by intraperitoneal injection. Anesthesia was maintained with isoflurane (1.5 to 2% in 100% O_2) for the duration of the surgery and subsequent recording period (SomnoSuite, Kent Scientific). Mouse internal temperature was monitored with a rectal probe and maintained at 35.5° to 37.5°C with a temperature controller (TC-344B, Warner Instruments) and thermoelectric heater (C3200-6145, Honeywell) embedded in castable cement (Aremco). The lumbar vertebral column was exposed and secured with custom spinal clamps (Mike's Machine, Attleboro, MA). Bone dorsal to the target DRG(s) (L3 to L5) was removed with rongeurs. The surgical site was continuously perfused with and immersed in external solution containing (in mM) 140 NaCl, 3.1 KCl, 0.5 KH_2PO_4, 6 glucose, 1.2 $CaCl_2$, 1.2 $MgSO_4$, and 10 HEPES. pH was adjusted to 7.4 with NaOH. The epineurium surrounding the DRG was removed with fine forceps. The DRG was visualized using custom reflective optics on an upright compound microscope (Zeiss). Cell bodies on the surface of the DRG were accessible for recording. Borosilicate glass pipettes (TW150F-4, WPI) were pulled to achieve a 20- to 30-μm tip diameter. Pipettes were then filled with external solution, and fluorescent cell bodies that were labeled with dye-conjugated CTB were targeted for cell-attached recordings.

Neuron receptive fields (RFs) were localized using a small paintbrush and gentle manual probing. For Meissner afferents, RFs were confined to single toe or pedal pad in the hindlimb. To estimate conduction velocity (CV), an electrical stimulus was delivered to the RF using a bipolar electrode. The delivered current was 2.5 times the threshold at which the neuron fired an action potential. CVs were estimated by dividing the conduction latency (average latency out of 10 trials) by the distance between the DRG and the RF. This distance did not account for the tortuosity of the sensory axon, and thus, the reported CVs are a lower bound on the true value. Force-controlled indentation of skin was achieved using an indenter (Model 300 C-I, Aurora Scientific) mounted on two orthogonal linear motorized stages (MTS25/M-Z8E, Thorlabs). The XY position of the indenter was controlled using the stages. The indenter was positioned on top of the RF such that the tip of the indenter was barely touching the surface of the glabrous pad. Sinusoidal force stimuli and low-pass filtered (15-ms boxcar) force steps were synthesized in MATLAB (Mathworks, Natick, MA) and delivered to the skin.

For random recordings of Aβ LTMRs that innervate glabrous skin (Fig. 1), the hindpaw glabrous skin pedal pads of $TrkB^{flox/flox}$ controls and $TrkB^{cKO}$ mice were injected with CTB conjugated to Alexa 488 24 to 72 hours before recording. Neurons with large soma diameters (>25 μm) that contained CTB 488 were targeted for recording. The receptive fields of the neurons were localized with manual brushing, and force indentations (0.5-s duration, 1- to 75-mN intensity) were applied to the receptive field. RA neurons were defined as those with spiking responses to indentation at only the onset or offset of the step indentation. SA neurons were defined as those with spikes occurring at the onset and the middle of the step indentation. SA neurons never increased their firing rate in response to the termination of the indentation. Nonresponsive (NR) neurons were defined as those that produced action potentials in response to stretching of the foot, but not to the indentation. Extracellular action potentials were recorded using a Multiclamp 700A amplifier (Axon Instruments) operating in the voltage-clamp configuration, which was constantly adjusted so that no current was passed by the amplifier. Electrophysiological data was digitized at 40 kHz by a 16-bit A/D converter (USB-6259, National Instruments), low-pass filtered at 10 kHz using the amplifier's internal four-pole Bessel filter, and acquired using pClamp. All electrophysiological data were analyzed using custom Python scripts.

Quantification of Meissner corpuscle and Merkel complex density

Images of serial sections of glabrous pads were sectioned at 25 μm. Images of sections were analyzed in the Fiji distribution of ImageJ (www.fiji.sc). In each section, the number of Meissner corpuscles, visualized by using S100 antibody (Meissner corpuscles formed large, ovoid masses in the dermal papillae compared to Schwann cells surrounding neurons, which are also $S100^+$), and the number of Merkel complexes, visualized by using TROMA-I antibody, were counted. Then, the length of the surface of the skin was traced and measured in ImageJ and multiplied by the thickness of the sections to obtain a volume in mm^3. Density was calculated by dividing the number of corpuscles or Merkel complexes (clusters of Merkel cells) by the volume of skin.

Behavior

Mice used for behavioral experiments were kept on a reversed light-dark cycle and were tested during the dark phase. Male mice of mixed genetic background (C57BL/6J and CD1) were ear notched for identification and genotyped at approximately P21. Females were not used because of potential effects of the estrous cycle on behavior and a preliminary observation that female mice have lower von Frey thresholds than male mice. Ear notching was performed using an ear punch device (Kent Scientific). Mice 6 to 16 weeks of age were subjected to behavioral tests. Mutant animals were compared to control littermates from the same genetic crosses to control for strain or genetic background variability. All behavioral testing was performed by an experimenter blind to genotype.

von Frey paw withdrawal test

For the von Frey paw withdrawal test, a sheet of wire mesh (9217T52, McMaster-Carr) was attached to an acrylic frame and positioned about 14 inches above a table. Mice were placed in 5-inch–by–2-inch clear, acrylic chambers, which were taped on top of the mesh. Before the test date, mice were habituated to the chambers for 1 hour for two consecutive days. On the test date, withdrawal responses were measured. After allowing the mice to habituate for 1 hour, von Frey filaments (North Coast Medical) were applied to the left hindpaw. The experimenter applied the filament onto or within close proximity to the pedal pads of the hindpaw. Care was taken to avoid the hairy skin in the middle of the hindpaw. Starting with the lowest force, each filament was applied five times in a row, followed by a brief break. Then, the filament was applied another five times for a total of 10 applications. The number of paw withdrawals was recorded for each filament weight.

Operant conditioning surgery and water restriction

Before operant conditioning, control $TrkB^{flox/flox}$ and mutant $TrkB^{cKO}$ mice were implanted with headplates in order to restrain them to the operant conditioning behavior apparatus. Adult (>P60) mice were anaesthetized with isoflurane (1.75 to 2% in O_2). Following removal of the scalp and periosteum, MetaBond dental cement was used to secure a lightweight, titanium headplate to the skull. Five days after surgery, mice began water restriction (40 ml/kg

of initial body weight) until they weighed 85% of their prerestriction weight. Animals were monitored for health conditions every training and testing day using a detailed health assessment adapted for water deprived mice (*39*). Health categories included weight, posture and grooming, activity level, signs of normal eating and waste elimination, and signs of dehydration. The minimum required daily water intake for each animal was 0.8 ml during data collection. Any animal that did not receive this much during the assay was supplemented up to the minimum volume.

Operant conditioning training

Mice were kept on a reversed light-dark cycle, and behavioral sessions were held daily for each animal. Behavioral paradigm control was performed by a custom written program running within the WaveSurfer application (Howard Hughes Medical Institute) in MATLAB. On the first and second days of training, each animal was given about 1 min to freely roam the apparatus platform. Mice were then habituated to the head restraint for 5 to 15 min with ad libitum water from the spout. To minimize the stress and movement of the animal, a three-sided acrylic enclosure was placed over the animal's body. On the third day of training, the right forepaw of each animal was secured over a 3-mm square hole in the apparatus platform, using an elastic strap over the forearm and clear cellophane tape over the back of the forepaw. A fine mechanical stimulator (Model 300 C-I, Aurora Scientific) positioned beneath the platform was used to apply a 75-mN step indentation stimulus to the glabrous skin of the forepaw. This indentation was applied atop a minimal force (<1 mN) used to hold the arm in position. If the animal licked the spout within 2 s of the stimulus onset, it received a 5-μl water reward. Over the next 2 weeks of training, the response period was reduced to 0.5 s, and a no-lick window of 3 s was introduced to discourage spurious licks. In the final phase of training, animals were presented with a range of stimulus amplitudes between 0.5 and 50 mN on 60% of trials, with 20% of all trials serving as no-stimulus (catch) trials, and 20% with a salient 75-mN stimulus to maintain task engagement. Within 3 weeks, animals exhibited stable psychometric functions, with average response rate of 80.5 ± 3.5% and false alarm rate of 17.1 ± 2.5% (mean ± SEM) for the 2 days preceding data collection. Mice displayed some differences in overall sensitivity between von Frey and operant conditioning. Differences in stimulus application—including probe diameter, stimulus waveform, and holding force—likely account for these sensitivity differences.

Operant conditioning data collection and sorting

For all animals, data was collected for 6 days, following a pattern of 2 days of testing blocks followed by 1 day of an easier training paradigm. To exclude data when animals were not engaged in the behavior task, blocks of trials characterized by overall poor performance were omitted from analysis of the detection threshold. We used a d′ statistic to identify these blocks of disengagement in the task, calculated using only trials with salient stimuli levels greater than 40 mN (Eq. 1).

$$d' = Z(\text{hit rate}) - Z(\text{false alarm rate}) \quad (1)$$

For the first and last 14 trials in a session, d′ was calculated over the entire block and the same value was assigned to each of the 14 trials. For all other trials in a session, d′ was calculated over blocks of 30 trials, and the value was assigned to the middle trial in the block (i.e., the d′ value for trial 15 was found using all stimulus trials over 40 mN between trials 1 and 30). Only blocks with at least 15 trials of d′ greater than or equal to 1.5 were used in data analysis. Animals with fewer than 750 viable trials were excluded.

To fit psychometric curves to the aggregate data, all stimulus trials were distributed into bins at 3-mN intervals, with the exception of the final bin with the most salient stimulus of 75 mN. For each animal, the average response rate during trials within each bin was calculated and averaged across all animals in either the control or $TrkB^{cKO}$ group. The MATLAB software package "psignifit 4" was used to fit a beta-binomial logistic sigmoid curve to each group (Eq. 2). Psignifit also output a parameter η that scaled the extra variance introduced within the bins of the data, where values near 1 indicated overdispersed data and values near 0 indicated good binomial dispersion.

$$\Psi(x; m, w, \lambda, \gamma) = \gamma + (1 - \lambda - \gamma)[11 + e^{-2\log(1.05-1)x - mw}] \quad (2)$$

where x is binned stimulus intensity, m is the midpoint of the psychometric function, w is the width of the curve, λ is the upper asymptote, and γ is the lower asymptote. Average psychometric threshold for each group was determined by fitting individual mouse response data to a beta-binomial logistic sigmoid curve using Psignifit. For each mouse, the force value at the midpoint of the psychometric function was determined to be its psychometric threshold. This data was then averaged within group.

Horizontal ladder assay

For the horizontal ladder assay, a ladder consisting of two parallel acrylic sheets as sides and equally spaced aluminum rods was mounted above a table. An angled mirror was positioned below the ladder to increase visibility of foot position. The lighting in the testing room was dim to eliminate visual input as much as possible. Mice were trained on the ladder during two consecutive habituation days. During habituation, mice were placed on one end of the ladder and were allowed to walk across the ladder toward a cage on the opposite end. Trials in which the mice paused for more than 5 s, turned around, or walked on the rim of the ladder rather than the rungs were immediately repeated. This continued until mice successfully crossed the ladder three times, but each mouse was subjected to no more than five total trials per day. On the third day, videos of the mice crossing the ladder were recorded, and the number of slips and time to cross the ladder were measured by an experimenter who was blinded to genotype. The average values of three successful trials were obtained for each animal.

Wire hang assay

For the wire hang assay, a 35-cm aluminum wire (~2.5 mm in diameter) was hung about 14 inches above a table using two aluminum columns attached to a base. Two paper plates were positioned on each end of the wire to prevent mice from moving to the columns. The mouse was placed in the center of the wire, and a cage with bedding was placed below the mouse to provide a cushioned landing area. For each mouse, the time from placement on the wire to falling was measured for three successful trials. Mice that remained on the wire for 90 s or longer were removed from the wire, and their time to fall was counted as 90 s. Additionally, trials in which mice fell instantly after placement on the wire were not counted as successful, and the trial was repeated.

Tactile prepulse inhibition (PPI) assay

Control and $TrkB^{cKO}$ mice were subjected to the tactile inhibition assay, a measure of hairy skin sensitivity, as described (*40*).

Sunflower seed handling measurements

Sunflower seed habituation in home cages: One week before testing animals were habituated to black oil sunflower seeds (Bio-Serv S5137-1 and Wagner's 76025) in their home cage by adding one to two tablespoons of seeds to the floor of the cage for five consecutive days. If animals did not recognize seeds as a food source, a teaspoon of seeds were cracked before adding to the cage floor.

Behavior chamber habituation and handling 2 days before sunflower seed testing was as follows: Animals were habituated to behavior room environment and investigator handling by undergoing tail inking on habituation day 1. To ink the tail, each animal was gently lifted and placed on the cage wire food hopper facing away from the investigator. With the tail firmly held midway from the tail base, a blue permanent soy-ink marker was rolled across the tail, forming parallel lines to indicate identifying ear notch number. Once inked, animals were

gently transferred back into the home cage to await test chamber habituation.

The test chamber was constructed of a black matte acrylic wall and three optically clear walls, 10 inches (*l*)–by–8 inches (*w*)–by–8 inches (*h*) and 0.25 inches thick, centered on a white matte acrylic floor under diffuse warm white light (2700 K). Three digital USB 2.0 CMOS video cameras mounted on camera sliders were positioned on each clear side of the test chambers. One additional overview camera was mounted directly above the test chamber.

Assay and behavioral measurements were as follows: Seeds were withheld from the home cage for 2 days before and during testing to encourage foraging and seed eating in the test chamber. During habituation days 1 and 2, animals were removed from the home cage and placed in an empty test chamber resting on the white matte acrylic floor. Each animal was given two to three seeds while freely exploring the test chamber for 20 min. After the free exploration period, animals were returned to their home cages. On testing day 3, animals were transferred from their home cage and placed in the test chamber and allowed to explore the chamber for 5 min. After acclimation, two to three seeds were placed on the floor of the test chamber and the seed eating activity was recorded. At the completion of the test, animals were removed from the test chamber and returned to their home cage. Chambers were reset and cleaned with unscented soapy water, wiped down with distilled water, and dried. Animals that failed to eat seeds after 20 min were returned to their home cage, and the test was rescheduled. This approach was repeated until each animal fully deshelled and consumed multiple seeds. Seeds that were partially shelled, partially consumed, or discarded were not counted. Behaviors were measured by defined seed deshelling and eating actions: (i) Seed peeling and deshelling—the act of grasping and holding the sunflower seed between the forepaws, clamping the upper and lower incisors into the shell surface, and applying downward force (dip) that pushed the shell away from the head and teeth toward the floor. This action resulted in a systematic peeling of the shell to expose the seed kernel. Animals unable to maintain a firm grip on or fully grasp the shell would typically adapt by touching, tapping, resting and/or bracing the seed against the floor between the forepaws. Animals also "tucked" the shell against their abdomen, holding the shell between the forepaws, clamping their upper and lower incisors onto the shell surface pulling their heads backward away from the shell and forepaws to peel off sections of the shell exposing the seed kernel. (ii) Touch-taps—the act of touching and/or holding and/or bracing the seed shell between the forepaws and the floor during seed peeling. (iii) Dip—the act of holding the seed shell between forepaws, clamping shell between incisors, and applying downward force to peel off sections of shell. (iv) Rotate—the act of or ability to change and/or manipulate shell orientation within the forepaws. (v) Rocking—the act of grasping the shell between the forepaws with shell firmly between incisors, using forepaws to "rock" the shell side to side between the incisors to bite into the shell to peel and expose the seed kernel.

For a table of resources used in the sunflower seed assay, see the supplementary materials.

Gait analysis

A recording setup based on a modified design of LocoMouse (*41*) was built for high-speed, automated analysis of mouse locomotion behavior. The dimensions of the transparent corridor used were 64.5 cm (*l*) by 4 cm (*w*) by 6 cm (*h*). Dark enclosures were situated on both ends of the corridor, and the animal freely moved between the two ends. Acquisition were triggered by infrared sensors during each epoch of corridor crossing. Two mirrors angled at 48° downward flanked the longitudinal axis of the corridor, which projected the side views of the animal to a camera below. A single high-speed camera (Bonito CL-400B/C 2320 × 700 pixels, Allied Vision, Exton, PA) captured simultaneous videos of the bottom view and two side views of the animal at 200 frames per second. Videos of the animal were compressed and analyzed offline using a convolutional neural network for postural tracking written in PyTorch and MATLAB (Mathworks, Natick, MA). Briefly, an hourglass network based on (*42*) was trained on 1000 expert annotated frames to simultaneously recognize the following body parts in the bottom and side views: nose, start and end of the tail, forepaws, and hind paws. The positions of body parts from all three perspectives were combined to generate a three-dimensional postural time series. A hidden Markov model was used to infer the start and the end of each gait cycle based on paw velocity. The following parameters were measured for each gait cycle: velocity, height, tail elevation, hind paw width, cadence, stride length, paw width, stand duration, and vertical and horizontal tail oscillation. A linear mixed effect model of the form Y ~ Intercept + Genotype + Sex + Genotype:Sex+ (1|Name) and ANOVA was used for statistical testing. In the case where velocity is considered as an independent variable, a model of the form Y ~ Intercept + Velocity + Genotype + Sex + Genotype:Sex + Velocity:Genotype + Velocity:Sex + (1|Name) was used instead.

Electron microscopy

Forepaw toe pads (ages P21 to P39) were excised and immersed in a glutaraldehyde-formaldehyde fixative for 1 hour at room temperature, further dissected, and subsequently fixed overnight at 4°C. Sample preparation was done as previously described (*28*). Ultrathin sections were cut at 40 to 60 nm and imaged using a JEOL 1200EX transmission electron microscope at 80-kV accelerating voltage. Images were cropped and adjusted with normalization to enhance contrast using Fiji/ImageJ. For corpuscles that were larger than the imaging field, montage of images was generated using TrakEM2 (*43*). Only sections close to the center of Meissner corpuscles were included for quantification. Axons that did not have apparent lamellar wrappings were not included. Two researchers, not involved in EM data collection and blind to genotypes, independently counted the number of lamellar wrappings around designated axons. The counts from both researchers were averaged for final analysis. Differences in lamellar wrapping counts per axon between these two researchers ranged from 0 to 5 wrappings.

Modeling

To find the mutual information between point stimulus location and neural population response, we assumed K possible point stimulus locations, denoted s, where each of them is equally likely to occur, that is, $p(s) = 1/K$ for all s. Furthermore, we assumed $M(\leq K)$ distinct neural population responses, denoted r, where response $r = m$ corresponds to n_m different point stimulus locations. Some locations might not have tactile receptors, such that $L = \sum_{m=1}^{M} n_m \leq K$. Overall, the set $\{n_1, \ldots, n_M\}$ determines the efficiency with which neural population responses encode tactile location.

To find the mutual information between point stimulus location s and neural population response r, we use $\mathrm{MI}(s;r) = \mathrm{H}(s) - \mathrm{H}(s|r)$, where $\mathrm{H}(s)$ is the entropy of stimulus locations, and $\mathrm{H}(s|r)$ is the conditional entropy, conditioned on a particular population response. Because of the uniform stimulus location distribution, we have $\mathrm{H}(s) = \log_2 K$. To find the conditional entropy, we observe that $p(s|r = m) = 1/n_m$ for all locations s that yield population response $r = m$, and $p(s|r = m) = 0$ otherwise. This results in

$$\mathrm{H}(s|r) = -\sum_s p(s) \sum_{m=1}^{M} p(s|r = m) \log_2 p(s|r = m) = -\sum_{m=1}^{M} \frac{n_m}{K} \log_2 \frac{1}{n_m}$$

where we have used the fact that each stimulus location corresponds to at most one population response. Overall, this yields the mutual information

$$\mathrm{MI}(s;r) = \log_2 K + \sum_{m=1}^{M} \frac{n_m}{K} \log_2 \frac{1}{n_m}$$

In this expression, n_m/K is the overall fraction of stimulus locations that evoke population response $r = m$, and $1/n_m$ is the probability of each stimulus location given this response.

To find the set $\{n_1, ..., n_M\}$ that maximizes the mutual information, we define the column vector $\vec{n} = (n_1, ..., n_M)^T$ and write the mutual information in vector form, $\mathrm{MI}(s;r) = \log_2 K + K^{-1}\vec{n}^T \log_2 1/\vec{n}$, where the last division is element-wise. We can then perform a constraint optimization on $\vec{n}$ with constraint $\vec{1}^T\vec{n} = L$, resulting in $n_m^* = L/M$ for all m. Thus, optimal coding (under the above assumptions) distributes the population responses evenly across stimulus locations. Furthermore, the mutual information increases with L, such that it is maximized if all stimulus locations yield a neural response (i.e., there are no gaps in the receptive fields), when $L^* = K$. Under these circumstances, the mutual information becomes $\mathrm{MI}(s;r) = \log_2 M$, providing an upper bound.

For nonoverlapped, square receptive fields, the number of distinct population responses M equals the number of neurons N. If these receptive fields tile the whole stimulus space evenly, then the associated mutual information is $\mathrm{MI}(s;r) = \log_2 N$. As the number of discriminable spaces is $2^{MI(s;r)} = N$, the number of efficiently discriminable spaces per neuron is $2^{MI(s;r)}/N = 1$.

For overlapped, square receptive fields, each stimulus location within the receptive field of two distinct neurons results in a distinct neural population response. Two nonoverlapped layers with $N/2$ equally sized square receptive fields that are offset against each other result in $4(N/2) = 2N$ distinct population responses (ignoring boundary effects, which become negligible for large N). These responses evenly tile the stimulus space if the offset is maximized, in which case $\mathrm{MI}(s;r) = \log_2 2N$. This results the number of efficiently discriminable space per neuron to be given by $2^{MI(s;r)}/N = 2$.

The two-point discrimination capability of square receptive fields was modeled by imagining a point stimulus presented to the center of a discriminable space and a circle of points presented at some distance d from the central point. The central point and the shifted point were presented asynchronously. For a given d, the fraction of the circle's circumference that extended outside the central discriminable space into a new discriminable space was considered the percent correct (i.e., the percentage of points unambiguously distinguishable from the central point). For nonoverlapped squares with side length s and with a central point presented within a single square

$$\%\ \text{correct} = \begin{cases} 0, & d \le \frac{s}{2} \\ 100\frac{4}{\pi}\cos^{-1}\frac{s}{2d}, & \frac{s}{2} < d \le \frac{s}{\sqrt{2}} \\ 100, & d < \frac{s}{\sqrt{2}} \end{cases}$$

For overlapped squares with side length $\sqrt{2}s$ and with a central point presented within a discriminable space:

$$\%\ \text{correct} = \begin{cases} 0, & d \le \frac{s}{2\sqrt{2}} \\ 100\frac{4}{\pi}\cos^{-1}\frac{s}{2\sqrt{2}d}, & \frac{s}{2\sqrt{2}} < d \le \frac{s}{2} \\ 100, & d < \frac{s}{2} \end{cases}$$

To model irregular and variable receptive fields, images of overlapped and nonoverlapped Voronoi tessellations were generated in MATLAB using the Voronoi function. The image set consisted of 4000 tessellations seeded with 84 to 101 random points in a square window. Number of neurons, N, for a single tessellation was the number of seeded points forming Voronoi cells that were within the window. Pairs of tessellations were overlapped to create 2000 overlapped mosaics with number of neurons equal to the combined number of neurons in the overlaid pairs. Mutual information between neural responses r and stimuli s was defined as above:

$$\begin{aligned} MI(s;r) &= H(s) - H(s|r) \\ &= \log_2 K + \sum\nolimits_{m=1}^{M} \frac{n_m}{K} \log_2 \frac{1}{n_m} \end{aligned}$$

where K is the total number of pixels and n_m are the number of pixels per discriminable space. Mutual information was normalized by the number of neurons ($2^{MI}/N$). The difference between overlapped and nonoverlapped Voronoi tessellations was determined to be statistically significant using 5000 bootstrap samples, each consisting of a randomly chosen pair from the 2000 overlapped tessellations and 2000 nonoverlapped tessellations.

Code availability

The computer code that supports the findings of this study is available from the corresponding author upon reasonable request.

Data availability

The data that support the findings of this study are available from the corresponding author upon reasonable request.

REFERENCES AND NOTES

1. R. Wagner, G. Meissner, Über das Vorhandensein bisher unbekannter eigenthümlicher Tastkörperchen (Corpuscula tactus) in den Gefühlswarzchen der menschlichen Haut and über die Endausbreitung sensitiver Nerven. *Nachricten von der Georg-August-Universität und der Königl Gesellschaft der Wissenschaften zu Göttingen* **2**, 17–30 (1852).
2. T. González-Martínez *et al*., Absence of Meissner corpuscles in the digital pads of mice lacking functional TrkB. *Brain Res.* **1002**, 120–128 (2004). doi: 10.1016/j.brainres.2004.01.003; pmid: 14988041
3. T. González-Martínez *et al*., BDNF, but not NT-4, is necessary for normal development of Meissner corpuscles. *Neurosci. Lett.* **377**, 12–15 (2005). doi: 10.1016/j.neulet.2004.11.078; pmid: 15722178
4. P. Perez-Pinera *et al*., Characterization of sensory deficits in *TrkB* knockout mice. *Neurosci. Lett.* **433**, 43–47 (2008). doi: 10.1016/j.neulet.2007.12.035; pmid: 18248898
5. S. da Silva *et al*., Proper formation of whisker barrelettes requires periphery-derived Smad4-dependent TGF-β signaling. *Proc. Natl. Acad. Sci. U.S.A.* **108**, 3395–3400 (2011). doi: 10.1073/pnas.1014411108; pmid: 21300867
6. Y. Liu *et al*., Sexually dimorphic BDNF signaling directs sensory innervation of the mammary gland. *Science* **338**, 1357–1360 (2012). doi: 10.1126/science.1228258; pmid: 23224557
7. L. Bai *et al*., Genetic identification of an expansive mechanoreceptor sensitive to skin stroking. *Cell* **163**, 1783–1795 (2015). doi: 10.1016/j.cell.2015.11.060; pmid: 26687362
8. C. Ma, D. F. Donnelly, R. H. LaMotte, In vivo visualization and functional characterization of primary somatic neurons. *J. Neurosci. Methods* **191**, 60–65 (2010). doi: 10.1016/j.jneumeth.2010.06.010; pmid: 20558205
9. W. Luo, H. Enomoto, F. L. Rice, J. Milbrandt, D. D. Ginty, Molecular identification of rapidly adapting mechanoreceptors and their developmental dependence on ret signaling. *Neuron* **64**, 841–856 (2009). doi: 10.1016/j.neuron.2009.11.003; pmid: 20064391
10. S. M. Maricich, K. M. Morrison, E. L. Mathes, B. M. Brewer, Rodents rely on Merkel cells for texture discrimination tasks. *J. Neurosci.* **32**, 3296–3300 (2012). doi: 10.1523/JNEUROSCI.5307-11.2012; pmid: 22399751
11. S. M. Maricich *et al*., Merkel cells are essential for light-touch responses. *Science* **324**, 1580–1582 (2009). doi: 10.1126/science.1172890; pmid: 19541997
12. K. M. Morrison, G. R. Miesegaes, E. A. Lumpkin, S. M. Maricich, Mammalian Merkel cells are descended from the epidermal lineage. *Dev. Biol.* **336**, 76–83 (2009). doi: 10.1016/j.ydbio.2009.09.032; pmid: 19782676
13. C. N. Perdigoto, E. S. Bardot, V. J. Valdes, F. J. Santoriello, E. Ezhkova, Embryonic maturation of epidermal Merkel cells is controlled by a redundant transcription factor network. *Development* **141**, 4690–4696 (2014). doi: 10.1242/dev.112169; pmid: 25468937
14. A. Ramirez *et al*., A keratin K5Cre transgenic line appropriate for tissue-specific or generalized Cre-mediated recombination. *Genesis* **39**, 52–57 (2004). doi: 10.1002/gene.20025; pmid: 15124227
15. N. F. Shroyer *et al*., Intestine-specific ablation of *mouse atonal homolog 1* (*Math1*) reveals a role in cellular homeostasis. *Gastroenterology* **132**, 2478–2488 (2007). doi: 10.1053/j.gastro.2007.03.047; pmid: 17570220
16. A. Van Keymeulen *et al*., Epidermal progenitors give rise to Merkel cells during embryonic development and adult homeostasis. *J. Cell Biol.* **187**, 91–100 (2009). doi: 10.1083/jcb.200907080; pmid: 19786578
17. L. Madisen *et al*., A robust and high-throughput Cre reporting and characterization system for the whole mouse brain. *Nat. Neurosci.* **13**, 133–140 (2010). doi: 10.1038/nn.2467; pmid: 20023653
18. M. Rutlin *et al*., The cellular and molecular basis of direction selectivity of Aδ-LTMRs. *Cell* **159**, 1640–1651 (2014). doi: 10.1016/j.cell.2014.11.038; pmid: 25525881
19. T. Uesaka, M. Nagashimada, S. Yonemura, H. Enomoto, Diminished *Ret* expression compromises neuronal survival in the colon and causes intestinal aganglionosis in mice. *J. Clin. Invest.* **118**, 1890–1898 (2008). doi: 10.1172/JCI34425; pmid: 18414682
20. L. Li *et al*., The functional organization of cutaneous low-threshold mechanosensory neurons. *Cell* **147**, 1615–1627 (2011). doi: 10.1016/j.cell.2011.11.027; pmid: 22196735
21. V. E. Abraira, D. D. Ginty, The sensory neurons of touch. *Neuron* **79**, 618–639 (2013). doi: 10.1016/j.neuron.2013.07.051; pmid: 23972592
22. A. Iggo, H. Ogawa, Correlative physiological and morphological studies of rapidly adapting mechanoreceptors in cat's glabrous skin. *J. Physiol.* **266**, 275–296 (1977). doi: 10.1113/jphysiol.1977.sp011768; pmid: 853451
23. W. D. Willis, R. E. Coggeshall, *Sensory Mechanisms of the Spinal Cord* (Kluwer Academic/Plenum Publishers, ed. 3, 2004), vol. 1.
24. K. O. Johnson, The roles and functions of cutaneous mechanoreceptors. *Curr. Opin. Neurobiol.* **11**, 455–461 (2001). doi: 10.1016/S0959-4388(00)00234-8; pmid: 11502392
25. A. G. Brown, R. E. Fyffe, R. Noble, Projections from Pacinian corpuscles and rapidly adapting mechanoreceptors of glabrous skin to the cat's spinal cord. *J. Physiol.* **307**, 385–400 (1980). doi: 10.1113/jphysiol.1980.sp013441; pmid: 7205669
26. L. M. Pubols, B. H. Pubols Jr.., Modality composition and functional characteristics of dorsal column mechanoreceptive afferent fibers innervating the raccoon's forepaw. *J. Neurophysiol.* **36**, 1023–1037 (1973). doi: 10.1152/jn.1973.36.6.1023; pmid: 4761717
27. P. Shortland, C. J. Woolf, Morphology and somatotopy of the central arborizations of rapidly adapting glabrous skin afferents in the rat lumbar spinal cord. *J. Comp. Neurol.* **329**, 491–511 (1993). doi: 10.1002/cne.903290406; pmid: 8454737

28. Q. Zhang, W. A. Lee, D. L. Paul, D. D. Ginty, Multiplexed peroxidase-based electron microscopy labeling enables simultaneous visualization of multiple cell types. *Nat. Neurosci.* **22**, 828–839 (2019). doi: 10.1038/s41593-019-0358-7; pmid: 30886406
29. W. R. Loewenstein, M. Mendelson, Components of receptor adaptation in a Pacinian corpuscle. *J. Physiol.* **177**, 377–397 (1965). doi: 10.1113/jphysiol.1965.sp007598; pmid: 14321486
30. B. M. Hooks, J. Y. Lin, C. Guo, K. Svoboda, Dual-channel circuit mapping reveals sensorimotor convergence in the primary motor cortex. *J. Neurosci.* **35**, 4418–4426 (2015). doi: 10.1523/JNEUROSCI.3741-14.2015; pmid: 25762684
31. T. C. Badea *et al*., New mouse lines for the analysis of neuronal morphology using CreER(T)/loxP-directed sparse labeling. *PLOS ONE* **4**, e7859 (2009). doi: 10.1371/journal.pone.0007859; pmid: 19924248
32. L. Madisen *et al*., Transgenic mice for intersectional targeting of neural sensors and effectors with high specificity and performance. *Neuron* **85**, 942–958 (2015). doi: 10.1016/j.neuron.2015.02.022; pmid: 25741722
33. H. Wu, J. Williams, J. Nathans, Morphologic diversity of cutaneous sensory afferents revealed by genetically directed sparse labeling. *eLife* **1**, e00181 (2012). doi: 10.7554/eLife.00181; pmid: 23256042
34. J. A. Gorski, S. R. Zeiler, S. Tamowski, K. R. Jones, Brain-derived neurotrophic factor is required for the maintenance of cortical dendrites. *J. Neurosci.* **23**, 6856–6865 (2003). doi: 10.1523/JNEUROSCI.23-17-06856.2003; pmid: 12890780
35. P. S. Danielian, D. Muccino, D. H. Rowitch, S. K. Michael, A. P. McMahon, Modification of gene activity in mouse embryos in utero by a tamoxifen-inducible form of Cre recombinase. *Curr. Biol.* **8**, 1323–1326 (1998). doi: 10.1016/S0960-9822(07)00562-3; pmid: 9843687
36. M. Jaegle *et al*., The POU proteins Brn-2 and Oct-6 share important functions in Schwann cell development. *Genes Dev.* **17**, 1380–1391 (2003). doi: 10.1101/gad.258203; pmid: 12782656
37. T. C. Badea, H. Cahill, J. Ecker, S. Hattar, J. Nathans, Distinct roles of transcription factors Brn3a and Brn3b in controlling the development, morphology, and function of retinal ganglion cells. *Neuron* **61**, 852–864 (2009). doi: 10.1016/j.neuron.2009.01.020; pmid: 19323995
38. S. Gong *et al*., A gene expression atlas of the central nervous system based on bacterial artificial chromosomes. *Nature* **425**, 917–925 (2003). doi: 10.1038/nature02033; pmid: 14586460
39. Z. V. Guo *et al*., Flow of cortical activity underlying a tactile decision in mice. *Neuron* **81**, 179–194 (2014). doi: 10.1016/j.neuron.2013.10.020; pmid: 24361077
40. L. L. Orefice *et al*., Peripheral mechanosensory neuron dysfunction underlies tactile and behavioral deficits in mouse models of ASDs. *Cell* **166**, 299–313 (2016). doi: 10.1016/j.cell.2016.05.033; pmid: 27293187
41. A. S. Machado, D. M. Darmohray, J. Fayad, H. G. Marques, M. R. Carey, A quantitative framework for whole-body coordination reveals specific deficits in freely walking ataxic mice. *eLife* **4**, e07892 (2015). doi: 10.7554/eLife.07892; pmid: 26433022
42. A. Newell, K. Yang, J. Deng, Stacked hourglass networks for human pose estimation. arXiv:1603.06937v2 [cs.CV] (26 July 2016).
43. A. Cardona *et al*., TrakEM2 software for neural circuit reconstruction. *PLOS ONE* **7**, e38011 (2012). doi: 10.1371/journal.pone.0038011; pmid: 22723842

ACKNOWLEDGMENTS

We thank E. Kuehn for AAV virus characterization, W.-C. Lee for providing access to ultramicrotomy equipment, and R. LaMotte and J. Woodbury for assistance with the in vivo physiological recording preparation. We thank M. Rutlin for preliminary analysis of behavioral deficits in *TrkB* conditional mutant mice, J. Barowski for help with figures, D. Paul for help with EM quantification, and T. Monteiro for technical assistance. We thank O. Mazor and P. Gorelik of the HMS Research Instrumentation Core Facility for consultation on operant conditioning design and MATLAB code and J. Huang for discussing unpublished sunflower seed handling measurements. We thank M. Pecot, S. Ashrafi, N. Sharma, and G. Fishell for helpful comments on the manuscript. **Funding:** N.L.N., M.W.S., Q.Z., and C.G. were Stuart H.Q. and Victoria Quan fellows at Harvard Medical School. This work was supported by NIH grants NS97344 (D.D.G.), NS105324 (A.J.E.), NS101843 (M.W.S), MH115554 (J.D.), K99 NS101057 (L.L.O.), and NS089521 (C.D.H.); NSF GRFP 2014177995 (M.W.S.); a scholar award by the James S. McDonnell Foundation (J.D.); and the Edward R. and Anne G. Lefler Center for Neurodegenerative Disorders (D.D.G.). D.D.G. is an investigator of the Howard Hughes Medical Institute. **Author contributions:** N.L.N., Y.L., A.J.E., and D.D.G. conceived the project; N.L.N. and Y.L. performed light microscopy experiments with assistance from A.A.; N.L.N., A.J.E., and B.P.L. did in vivo electrophysiological recordings with guidance from C.D.H.; M.W.S., M.I., J.R., and S.J.K. performed the operant conditioning behavioral experiments; L.L.O. performed the PPI experiments; C.G. and M.M.D. performed gait analysis with guidance from W.R.; N.L.N., A.A., and M.M.D. performed all other behavioral experiments; N.L.N. and J.D. performed the modeling; A.H., Q.Z., and S.J.C. did the EM analysis; N.L.N. and D.D.G. wrote the first draft of the paper, with sections subsequently provided by A.J.E.; and all authors contributed to the final manuscript draft. **Competing interests:** The authors have no competing interests. **Data and materials availability:** All data are available in the manuscript or the supplementary materials. The mouse strains generated for and used in this study are available from the corresponding author under a material agreement with Harvard.

SUPPLEMENTARY MATERIALS

science.sciencemag.org/content/368/6497/eabb2751/suppl/DC1
Supplementary Text
Figs. S1 to S10
MDAR Reproducibility Checklist
Movies S1 and S2

View/request a protocol for this paper from *Bio-protocol*.

12 February 2020; accepted 28 April 2020
10.1126/science.abb2751

Science

Meissner corpuscles and their spatially intermingled afferents underlie gentle touch perception

Nicole L. Neubarth, Alan J. Emanuel, Yin Liu, Mark W. Springel, Annie Handler, Qiyu Zhang, Brendan P. Lehnert, Chong Guo, Lauren L. Orefice, Amira Abdelaziz, Michelle M. DeLisle, Michael Iskols, Julia Rhyins, Soo J. Kim, Stuart J. Cattel, Wade Regehr, Christopher D. Harvey, Jan Drugowitsch and David D. Ginty

Science **368** (6497), eabb2751.
DOI: 10.1126/science.abb2751

Secrets of Meissner corpuscles

The Meissner corpuscle, a mechanosensory end organ, was discovered more than 165 years ago and has since been found in the glabrous skin of all mammals, including that on human fingertips. Although prominently featured in textbooks, the function of the Meissner corpuscle is unknown. Neubarth *et al.* generated adult mice without Meissner corpuscles and used them to show that these corpuscles alone mediate behavioral responses to, and perception of, gentle forces (see the Perspective by Marshall and Patapoutian). Each Meissner corpuscle is innervated by two molecularly distinct, yet physiologically similar, mechanosensory neurons. These two neuronal subtypes are developmentally interdependent and their endings are intertwined within the corpuscle. Both Meissner mechanosensory neuron subtypes are homotypically tiled, ensuring uniform and complete coverage of the skin, yet their receptive fields are overlapping and offset with respect to each other.

Science, this issue p. eabb2751; see also p. 1311

Science (print ISSN 0036-8075; online ISSN 1095-9203) is published by the American Association for the Advancement of Science, 1200 New York Avenue NW, Washington, DC 20005. The title *Science* is a registered trademark of AAAS.

science.sciencemag.org/content/368/6497/eabb2751/suppl/DC1

Supplementary Materials for

Meissner corpuscles and their spatially intermingled afferents underlie gentle touch perception

Nicole L. Neubarth*, Alan J. Emanuel*, Yin Liu*, Mark W. Springel, Annie Handler, Qiyu Zhang, Brendan P. Lehnert, Chong Guo, Lauren L. Orefice, Amira Abdelaziz, Michelle M. DeLisle, Michael Iskols, Julia Rhyins, Soo J. Kim, Stuart J. Cattel, Wade Regehr, Christopher D. Harvey, Jan Drugowitsch, David D. Ginty†

*These authors contributed equally to this work.
†Corresponding author. Email: david_ginty@hms.harvard.edu

Published 19 June 2020, *Science* **368**, eabb2751 (2020)
DOI: 10.1126/science.abb2751

This PDF file includes:

Other Supporting Online Material for this manuscript includes the following:
(available at science.sciencemag.org/content/368/6497/eabb2751/suppl/DC1)

Supplementary Text

Resources table for sunflower seed assay

REAGENT or RESOURCE	SOURCE	IDENTIFIER
GRAPHPAD Prism 8	GraphPad Software 7825 Fay Avenue, Suite 230 La Jolla, CA 92037 USA Phone: 858-454-5577 Fax: 858-454-4150 sales@graphpad.com support@graphpad.com	
IC Capture Video Acquisition Software	The Imaging Source, LLC Suite 400 6926 Shannon Willow Rd Charlotte, NC 28226 United States Phone: 704-370-0110 https://www.theimagesource.com/	
Stoelting Digital USB 2.0 CMOS Camera	Stoelting Co. 620 Wheat Lane, Wood Dale, IL 60191 T: 630.860.9700 F: 630.860.9775 E: info@stoeltingco.com www.stoeltingco.com	Camera: 60516 Vari-focal, 2.8-12mm Lens: 60528
Bio-Serv Black Oil Sunflower Seeds	Bio-Serv 3 Foster Lane Flemington, NJ 08822 US Phone: 800-996-9908 https://www.bio-serv.com/	S5137-1
Wagner's Four Season Oil Sunflower Seed	Wagner's, LLC P.O. Box 54 Jericho, N.Y. 11753 Phone: 516-933-6580 Fax: 516-933-6581 info@wagners.com	76025
Sunflower Seed Test Chamber Black Matte, Optically Clear Acrylic 0.25in, 10in(l) × 8in(w) × 8in(h)	Altec Plastics Inc. 116 B Street South Boston, MA 02127 617.269.1400 info@altecplastics.com https://shop.altecplastics.com/	

Sunflower Seed Floor, White Matte Acrylic 0.25in 36in(l) × 26in(w)	Altec Plastics Inc. 116 B Street South Boston, MA 02127 617.269.1400 info@altecplastics.com https://shop.altecplastics.com/	

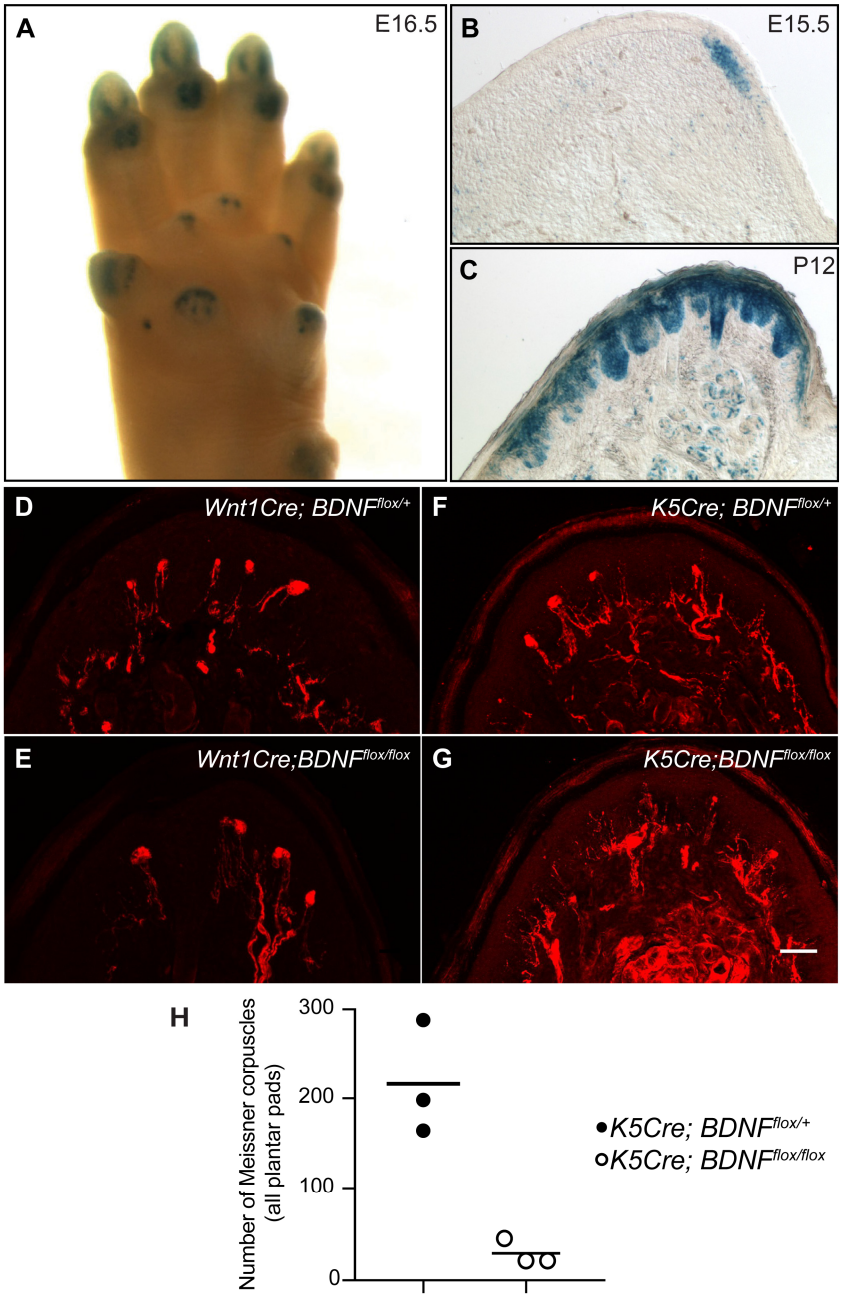

Fig. S1. BDNF expressed in epithelial cells, but not in neural crest-derived sensory neurons or Schwann cells, is essential for Meissner corpuscle formation.

A. Whole forelimb of an E16.5 *BDNF*^{lacZ} embryo stained using X-gal.

B-C. Forelimb palmar pad sections of *BDNF*^{lacZ} mice at E15.5 and P12 stained with X-gal.

D-G. Hindlimb plantar pad sections were stained with anti-S100 to reveal Meissner corpuscles

in *Wnt1Cre; BDNF$^{flox/flox}$* mice, in which BDNF expression is eliminated in DRG sensory neurons and Schwann cells, and control mice. The number of Meissner corpuscles in glabrous skin of control and *Wnt1Cre; BDNF$^{flox/flox}$* mice are comparable, and this comparison was done with two pairs of control (105 and 133 corpuscles in two hindlimb pedal pads per mouse) and *Wnt1Cre; BDNF$^{flox/flox}$* mice (119 and 89 corpuscles in two hindlimb pedal pads per mouse). (scale bar = 50 μm)

H. Quantifications of the number of Meissner corpuscles in all hindlimb plantar pads of *K5Cre; BDNF$^{flox/flox}$* mice, in which BDNF expression is eliminated in skin epithelial cells, and control mice at P20 (3 mice for each genotype, 6 hindlimb pedal pads per mouse). Black bars represent means. Serial sections were cut throughout the whole plantar region and Meissner corpuscles were identified by S100 staining and counted across all sections.

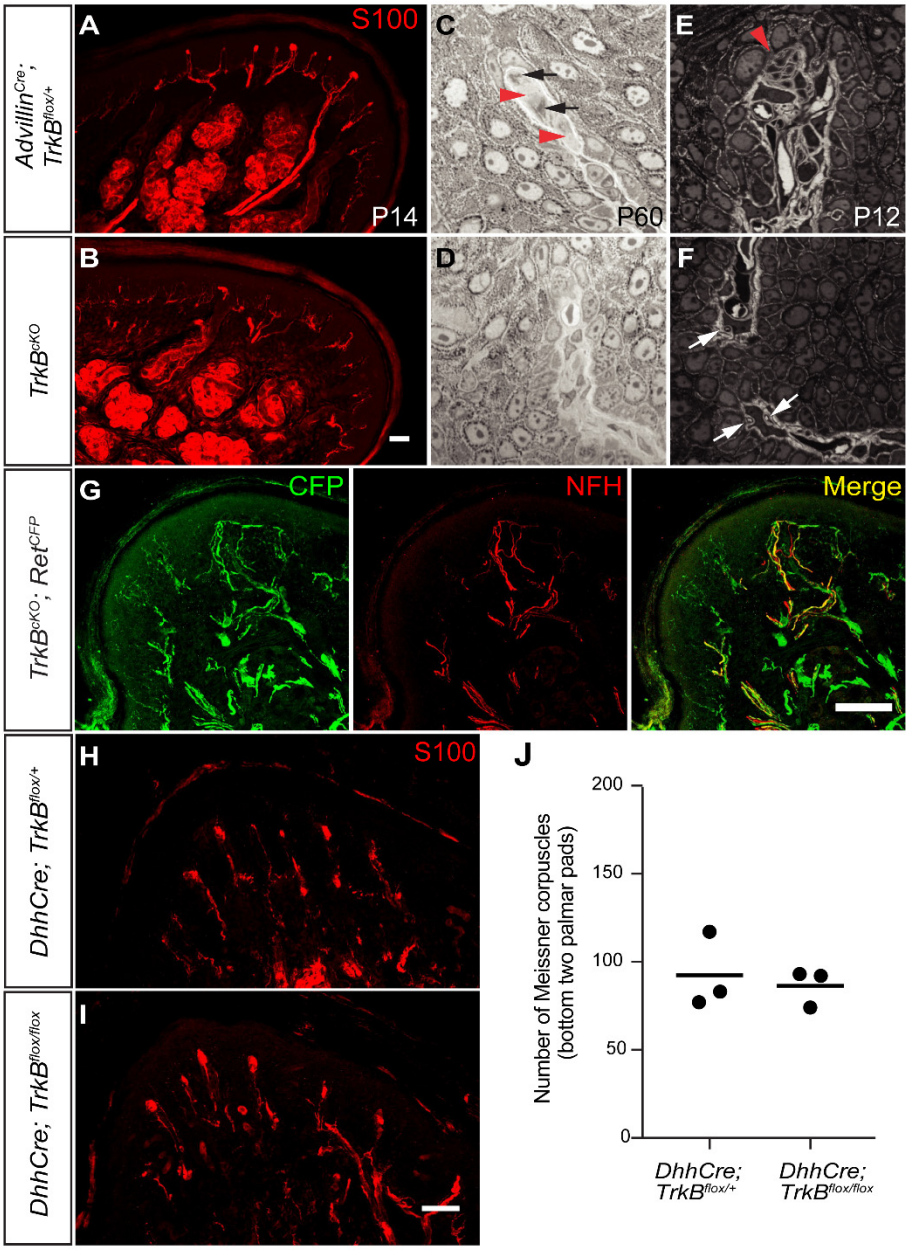

Fig. S2. TrkB is required in sensory neurons, but not glia cells, for the formation of Meissner corpuscles and their innervating sensory neurons.

A-B. Hindlimb plantar pad sections of control and *TrkB*^{cKO} mice at P14 stained with anti-S100 antibody. (scale bar = 50 µm)

C-F. To exclude the possibility that in sensory-neuron-specific *TrkB*^{cKO} mice Meissner corpuscles

are formed but fail to express S100 protein, we performed toluidine/methylene blue staining on semi-thin sections of the glabrous skin. Semi-thin sections (0.5 µm) of hindlimb plantar pads of control and *TrkB*^{cKO} mice were cut parallel to the skin surface. In C and D, mice were sacrificed at P60, and staining was done with methylene blue. Red arrowheads: cytoplasmic processes of lamellar cells; black arrows: nerve terminals (densely stained). In E and F, mice were sacrificed at P12, and staining was performed with toluidine blue. Red arrowheads: pre-mature corpuscle, white arrows: large caliber nerve fibers. No Schwann cells were observed in the dermal papillae of adult or P12 *TrkB*^{cKO} mice. These experiments were performed in 2 animals per age with similar results.

G. A forelimb palmar pad section of a P14 *TrkB*^{cKO}*; Ret*^{CFP} mouse stained with anti-GFP and anti-NFH antibodies. The majority of the NFH^{+} fibers present in glabrous skin dermal papillae at P14 are CFP^{+}. This experiment was performed in 2 mice with similar results. (scale bar = 50 µm)

H-I. Hindlimb plantar pad sections of control and *DhhCre; TrkB*$^{flox/flox}$ mice at P20 stained with anti-S100 antibody. *DhhCre* mice express Cre recombinase in all Schwann cells. (scale bar = 50 µm)

J. Quantification of the number of Meissner corpuscles in control and *DhhCre; TrkB*$^{flox/flox}$ mice at P20. Meissner corpuscles in the bottom two palmar pads of each forelimb were counted (3 mice for each genotype). Black bars represent means.

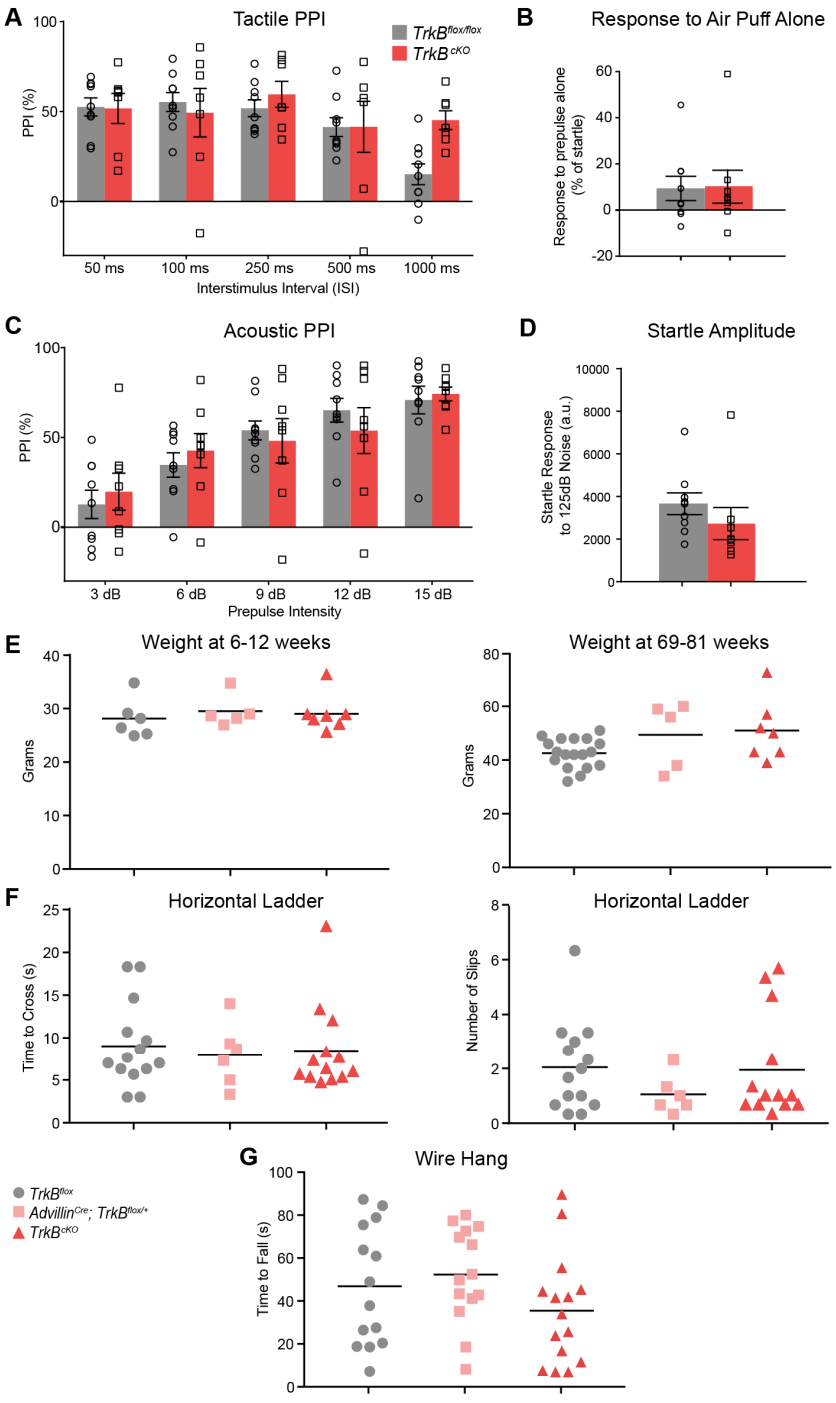

Fig. S3. *TrkB*^{cKO} mice have normal hairy skin sensitivity and are overtly normal.

A. Percent inhibition of the startle response to a 125-dB noise (pulse), when the startle noise was preceded by a light air puff (prepulse, 0.9 PSI, 50 ms) applied to the back hairy skin at

multiple inter-stimulus intervals (ISIs) between the prepulse and the pulse, for *TrkB*^{cKO} mutant mice and control littermates. Repeated measures, two-way ANOVA: no significant differences between genotypes.

B. Response to a light air puff (0.9 PSI, 50 ms) applied to the back hairy skin, for *TrkB*^{cKO} mutant mice and control littermates. Responses are expressed as a percent of startle response to a 125-dB noise. Student's t-test, not significant. N= 9 (control littermates) and 8 (*TrkB*^{cKO} mutants).

C. Percent inhibition of the startle response to a 125-dB noise (pulse), when the startle noise is preceded by a non-startling tone prepulse (80 dB for 20 ms, with a 100 ms ISI) in *TrkB*^{cKO} mutant mice and control littermates. Repeated measures, two-way ANOVA: no significant differences between genotypes.

D. Magnitude of startle response to a 125-dB noise in *TrkB*^{cKO} mutant mice and control littermates. Student's t-test, not significant.

E. Left: Weights of adult (6-12 weeks old) male control and *TrkB*^{cKO} mice are similar. Right: Weights of aged adult (69-81 weeks old) control and *TrkB*^{cKO} mice are also similar. Black bars represent means.

F *TrkB*^{cKO} mice performed similarly to controls when crossing a horizontal ladder. Each point represents the average of three trials for each animal, and black bars represent means.

G. *TrkB*^{cKO} mice performed similarly to controls when hanging from a suspended wire. Each point represents the average of three trials for each animal, and black bars represent means.

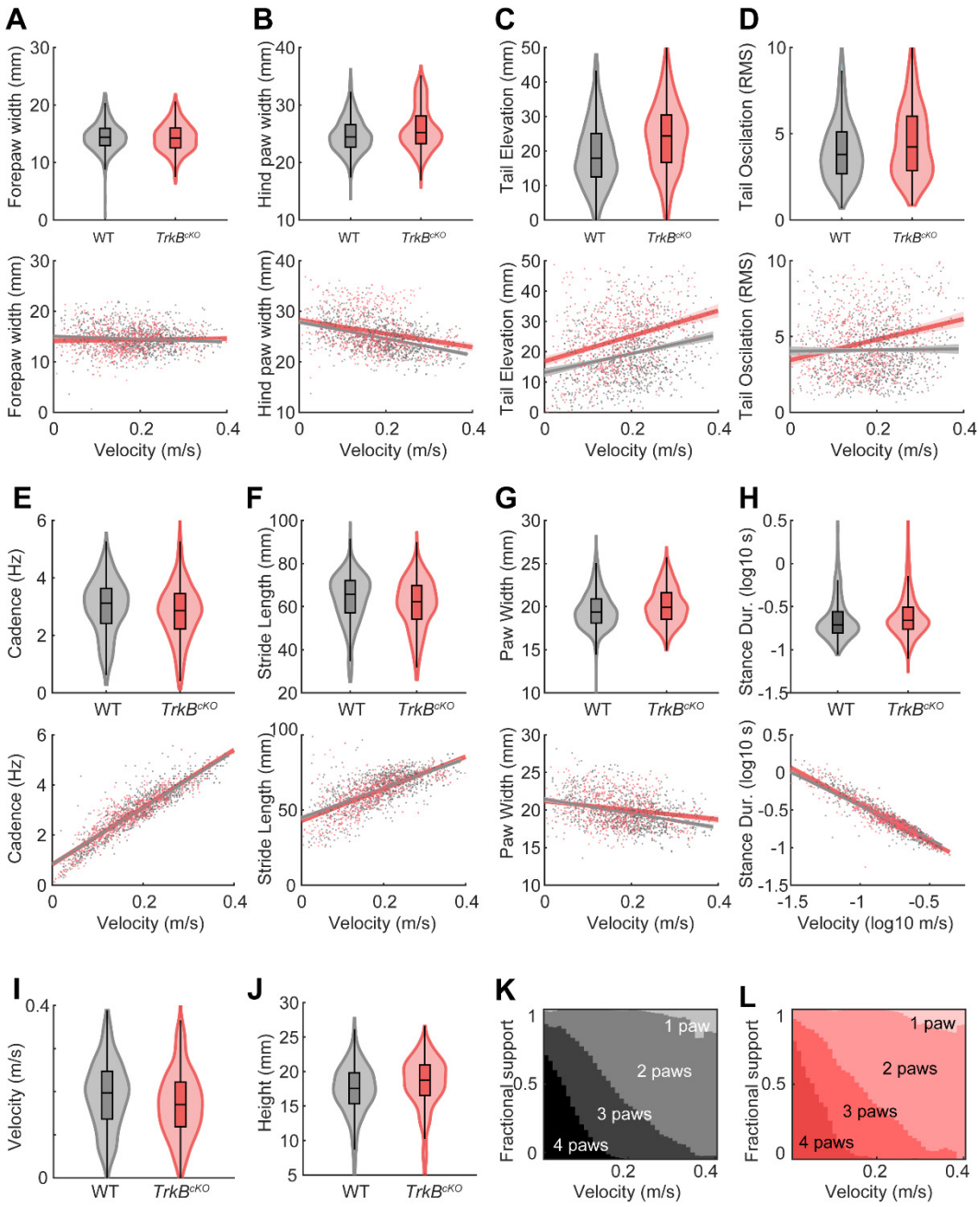

Fig. S4. *TrkB^{cKO}* mice have normal gait but more tail oscillation is observed at higher velocity.

A-H. Violin plots (top) and regression analyses with velocity as an independent variable (bottom) for animal forepaw width (A), hindpaw width (B), tail elevation (C), tail oscillation (D), cadence (E), stride length (F), paw width (contralateral forepaw to hindpaw) (G), average stance duration (H) for control mice in grey and *TrkB^{cKO}* mice in red.

I-J. Violin plots for velocity (I) and height (J)

K-L. Fraction of time during a single gait cycle for a given velocity when the subject had four (darkest) to one (lightest) paws on the floor for support. Control mice in grey and *TrkB*^{cKO} mice in red.

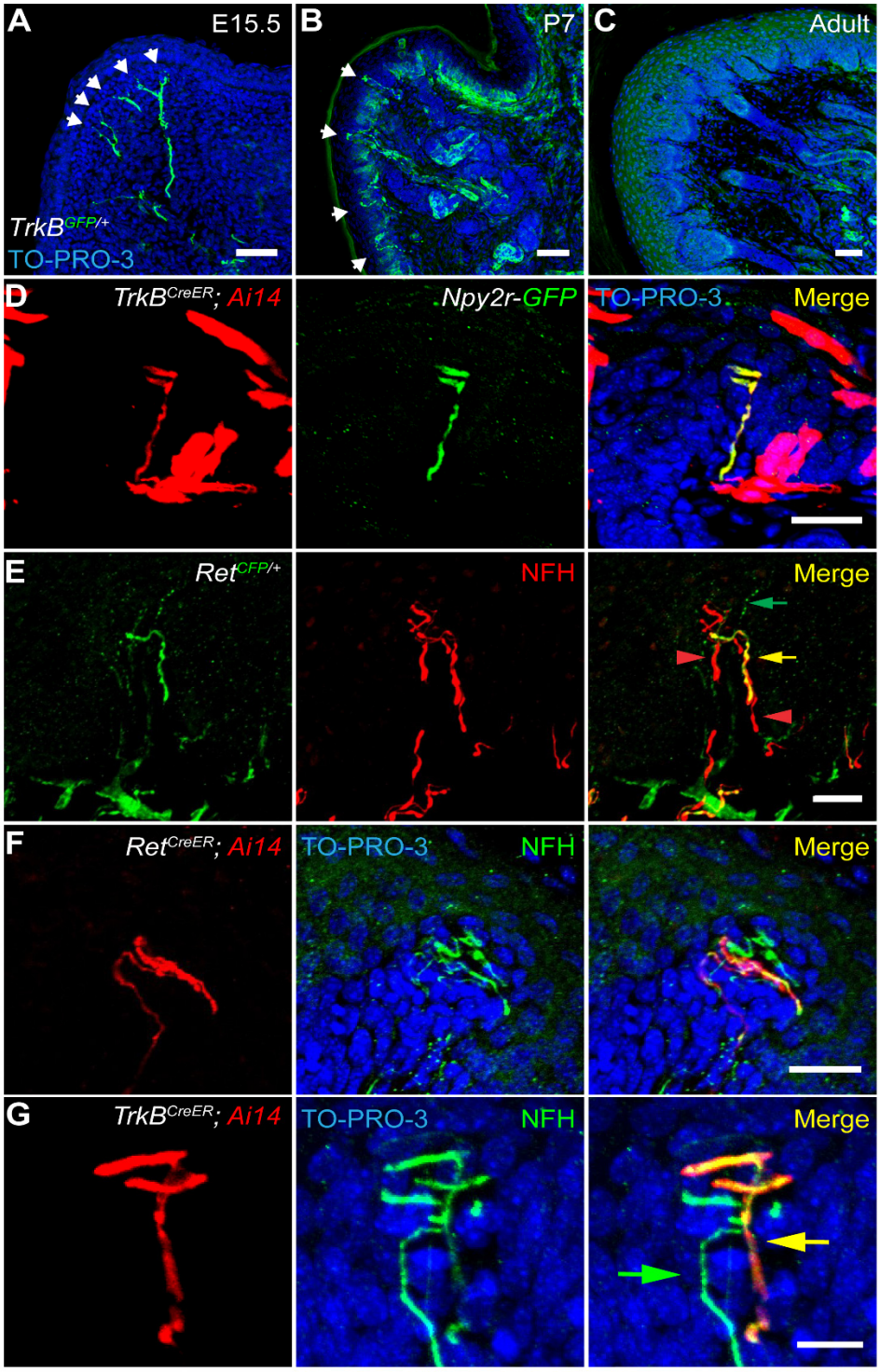

Fig. S5. TrkB$^+$ and Ret$^+$ neurons innervating Meissner corpuscles are distinct populations of neurofilament-positive afferents.

A-C. Forelimb palmar pad sections of *TrkB^{GFP}* mice at different developmental stages stained

with anti-GFP and TO-PRO-3. Note that GFP is expressed in Meissner corpuscle afferents at an early age (P7), but not in adults. These experiments were performed in multiple animals with similar results (A: 2 mice, B: 4 mice, C: 2 mice). (scale bar = 50 μm)

D. Glabrous skin section of a P20 *TrkB^{CreER}; Ai14; Npy2r-GFP* mouse treated with tamoxifen at P5 to permanently label early TrkB^{+} neurons. Section was stained with anti-DsRed, anti-GFP, and TO-PRO-3. Result observed in 6 corpuscles of 1 mouse. (scale bar = 25 μm)

E. A hindlimb digital pad section of a P50 *Ret^{CFP}* mouse stained with anti-GFP and anti-NFH antibodies. This experiment was performed in 3 mice with similar results. Yellow arrow: CFP^{+}/NFH^{+} Ret fiber. Green arrow: CFP^{+}/NFH^{-} nonpeptidergic C-fiber. Red arrowheads: NFH^{+}/CFP^{-} fibers. (scale bar = 25 μm)

F. Forelimb pedal pad section of a P20 *Ret^{CreER}; Ai14* mouse treated with tamoxifen at E10.5-E11.5. Section was stained with anti-NFH antibody and TO-PRO-3. This experiment was performed in 2 mice with similar results. (scale bar = 25 μm)

G. A hindlimb digital pad section of a P50 *TrkB^{CreER}; Ai14* mouse treated with tamoxifen at E16.5 (same mouse as used in Figure 3B). Section was stained with anti-DsRed, anti-NFH, and TO-PRO-3. This experiment was performed in 3 mice with similar results. (scale bar = 12.5 μm).

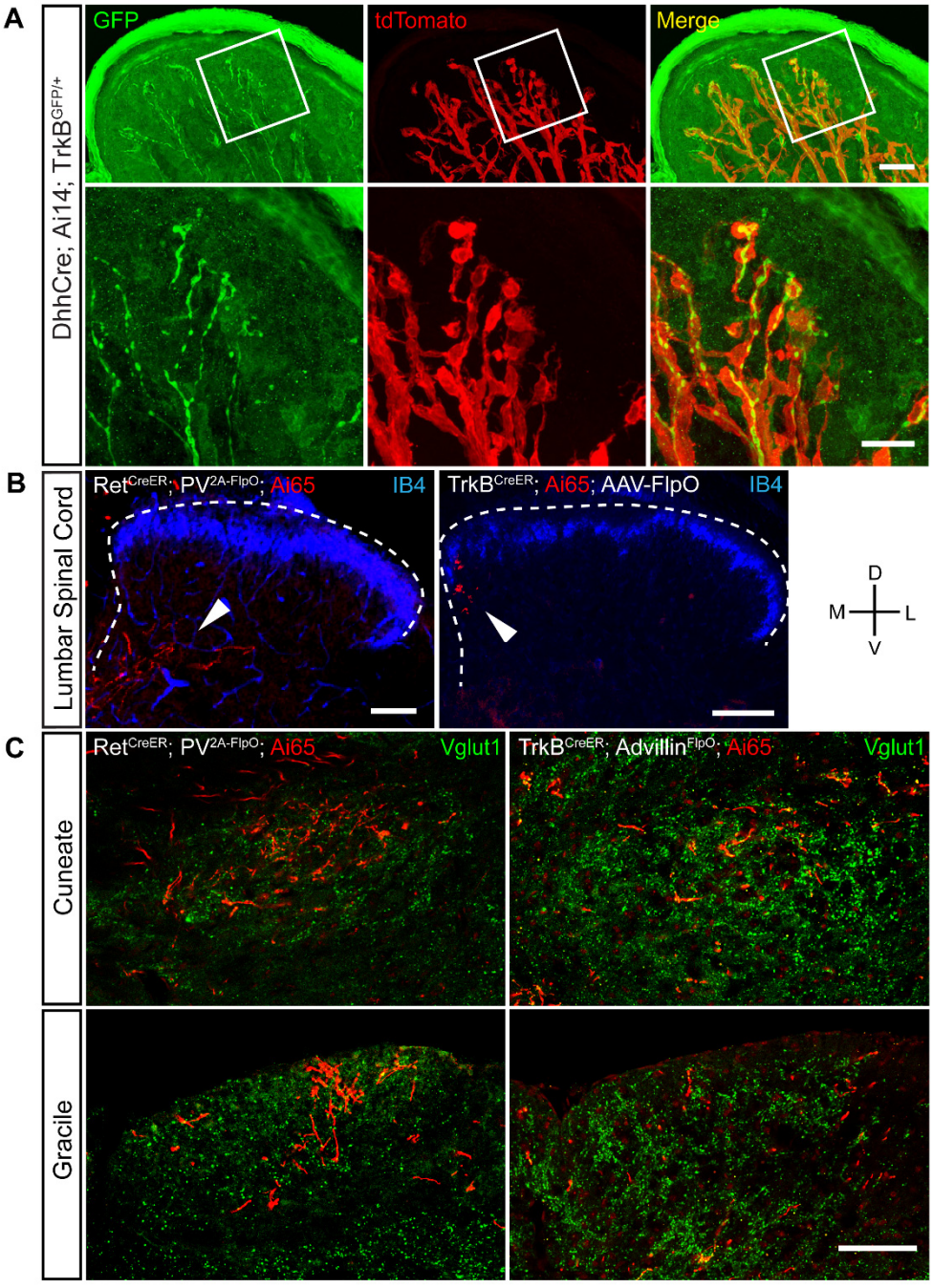

Fig. S6. Schwann cells are associated with TrkB-expressing fibers in dermal papillae during development and both TrkB$^+$ and Ret$^+$ Meissner corpuscle afferents form projections in the spinal cord and DCN.

A. Upper panels: A forelimb palmar pad section of a P5 *DhhCre; TrkB^{GFP}; Ai14* mouse stained with anti-GFP antibody. Schwann cells have not yet differentiated into lamellar cells at this age. TdTomato, which is expressed in Schwann cells, was detected via direct fluorescence. For each GFP^{+} fiber in dermal papillae, there are Schwann cell(s) associated with its tip. Lower panels: enlarged views of the region cropped in upper panels. This experiment was performed in 3 mice with similar results. (scale bars = 50 µm)

B. Transverse sections of lumbar spinal cords. Left panel is from a P21 *Ret^{CreER}; PV$^{2A\text{-}FlpO}$; Rosa26$^{LSL\text{-}FSF\text{-}tdTomato}$* (*Ai65)* mouse treated with tamoxifen at E11.5 and E12.5 (similar results were observed in three mice), and right panel is from an adult *TrkB^{CreER}; Ai65* mouse treated with tamoxifen at P5 and given an injection of AAV-FlpO to a glabrous hindlimb pedal pad to achieve labeling of a single TrkB^{+} Meissner afferent (a second section from this animal and sections from the other three animals are in Figure S6). Both sections were stained with anti-DsRed antibody and IB4. Arrowheads indicate dorsal horn collaterals. (scale bars = 100 µm, D = dorsal, V = ventral, M = medial, L = lateral)

C. Transverse sections of the medulla at the level of the cuneate and gracile nuclei of the DCN. Left panels are from a P21 *Ret^{CreER}; PV$^{2A\text{-}FlpO}$; Ai65* mouse treated with tamoxifen at E11.5 and E12.5 (DCN innervation observed in 3/3 mice), and right panels are from a P23 *TrkB^{CreER}; Advillin^{FlpO}; Ai65* mouse treated with tamoxifen at E13.5 and E14.5 (DCN innervation observed in this mouse and another adult mouse given tamoxifen at P4). All sections were stained with anti-Vglut1 and anti-DsRed antibodies. (scale bar = 100 µm; D = dorsal, V = ventral, M = medial, L = lateral)

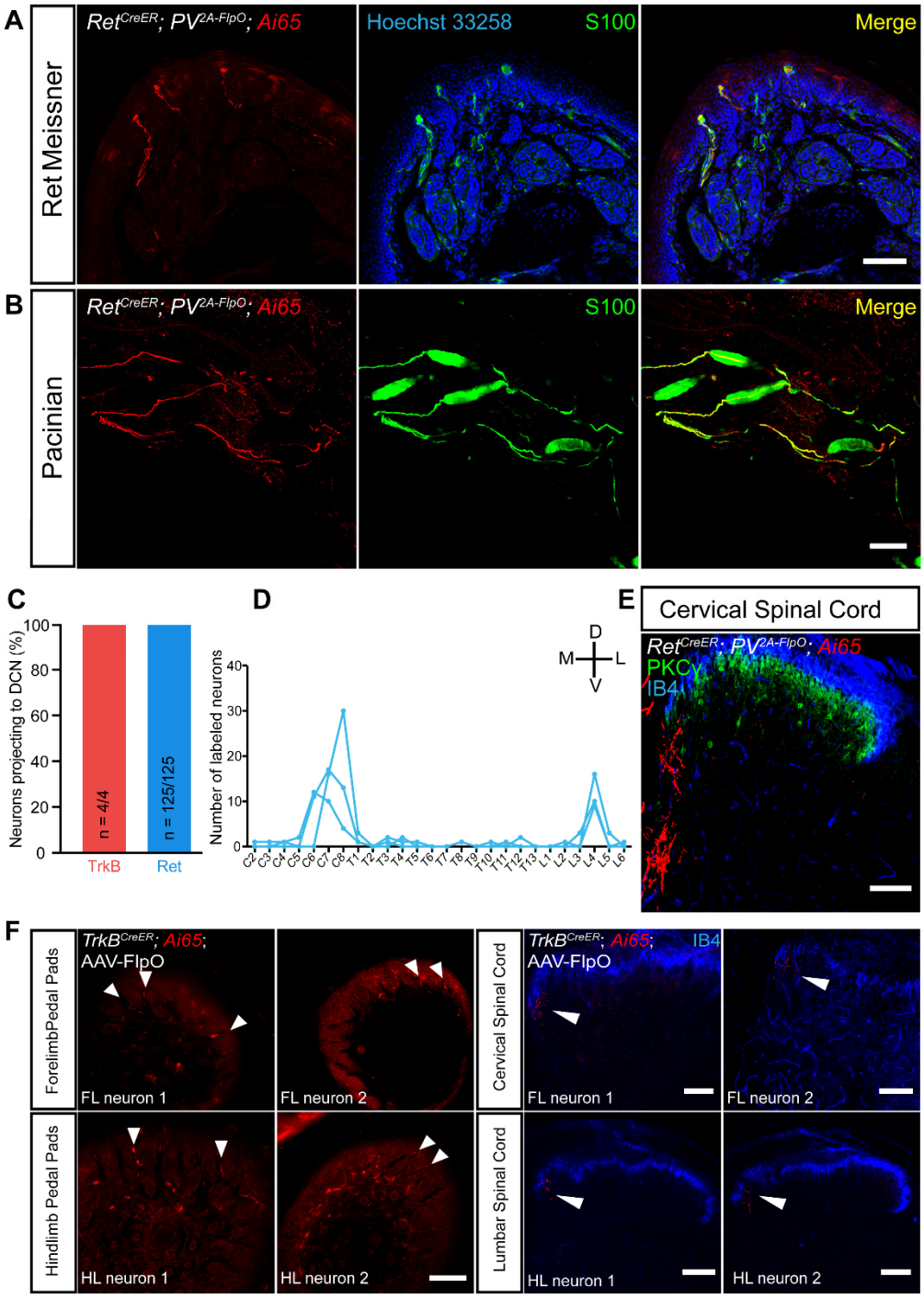

Fig. S7. TrkB⁺ and Ret⁺ Meissner corpuscle afferents display typical Aβ-LTMR morphology in the central nervous system.

A-B. A Ret-parvalbumin intersectional genetic strategy predominantly labels Ret$^+$ neurons innervating Meissner and Pacinian corpuscles. No tdTomato$^+$ neurons were observed in back and hindlimb hairy skin or in proprioceptors of the anterior tibialis muscle. A is a digital pad section from a P21 *Ret^{CreER}; PV$^{2A\text{-}FlpO}$; Ai65* mouse treated with tamoxifen at E11.5 and E12.5. Anti-S100 antibody labels Meissner corpuscles in the dermal papillae and Schwann cells surrounding the innervating sensory neurons. B is whole-mount immunostaining of Pacinian corpuscles located in the periosteum of the fibula from a *Ret^{CreER}; PV$^{2A\text{-}FlpO}$; Ai65* mouse. Anti-S100 antibody labels Pacinian corpuscles and Schwann cells surrounding the innervating sensory neurons. Skin sections and whole-mount Pacinian corpuscles were stained with anti-DsRed antibody. This experiment was performed in 3 mice with similar results. (scale bars = 100 μm).

C. Percentage of TrkB$^+$ pedal pad Meissner neurons traveling to the DCN via the dorsal columns at the transition between cervical spinal levels and the medulla (4/4 neurons from 4 *TrkB^{CreER}; Ai65* mice with AAV-FlpO injection into the pedal pads, 2 hindlimb and 2 forelimb), and percentage of Ret$^+$/PV$^+$ neurons (Pacinian and Meissner afferents, see Figure S6) traveling to the DCN (number of neurons in the dorsal column at the medulla was compared to number of fluorescent neurons in the DRG, 2 *Ret^{CreER}; PV$^{2A\text{-}FlpO}$; Ai65* mice, 76/76 and 49/49 neurons labeled in the DRG, respectively). Note that the dual genetic/paw virus injection strategy has a low labeling efficiency and marks few neurons per animal.

D. Number of tdTomato$^+$ neurons in the DRG per spinal segment in three *Ret^{CreERT2}; PV$^{2A\text{-}FlpO}$; Ai65* mice. This is consistent with the finding that the Ret-PV intersectional strategy

predominantly labels limb-level Pacinian afferents and Meissner afferents innervating glabrous skin.

E. Transverse section of cervical spinal cord from a P21 *Ret^{CreER}; PV$^{2A\text{-}FlpO}$; Ai65* mouse treated with tamoxifen at E11.5 and E12.5. Section was stained with anti-DsRed, anti-PKCγ, and IB4. This experiment was performed in 3 mice with similar results. (scale bar = 100 µm; D = dorsal, V = ventral, M = medial, L = lateral)

F. Peripheral terminations in the glabrous skin (arrowheads, left panels) and example spinal cord collateral morphologies (arrowheads, right panels) for single forelimb (FL) and hindlimb (HL) pedal pad neurons in adult *TrkB^{CreER}; Ai65* mice treated with tamoxifen at P5 and given an injection of AAV-FlpO to a glabrous pedal pad in order to achieve sparse labeling of a single neuron per animal. Whole-mount pedal pads were stained with anti-dsRed. Spinal cord sections were cut transversely and stained with IB4 and anti-dsRed. Another spinal cord section from HL neuron 1 is depicted in Figure S5. (scale bars = 100 µm; D = dorsal, V = ventral, M = medial, L = lateral)

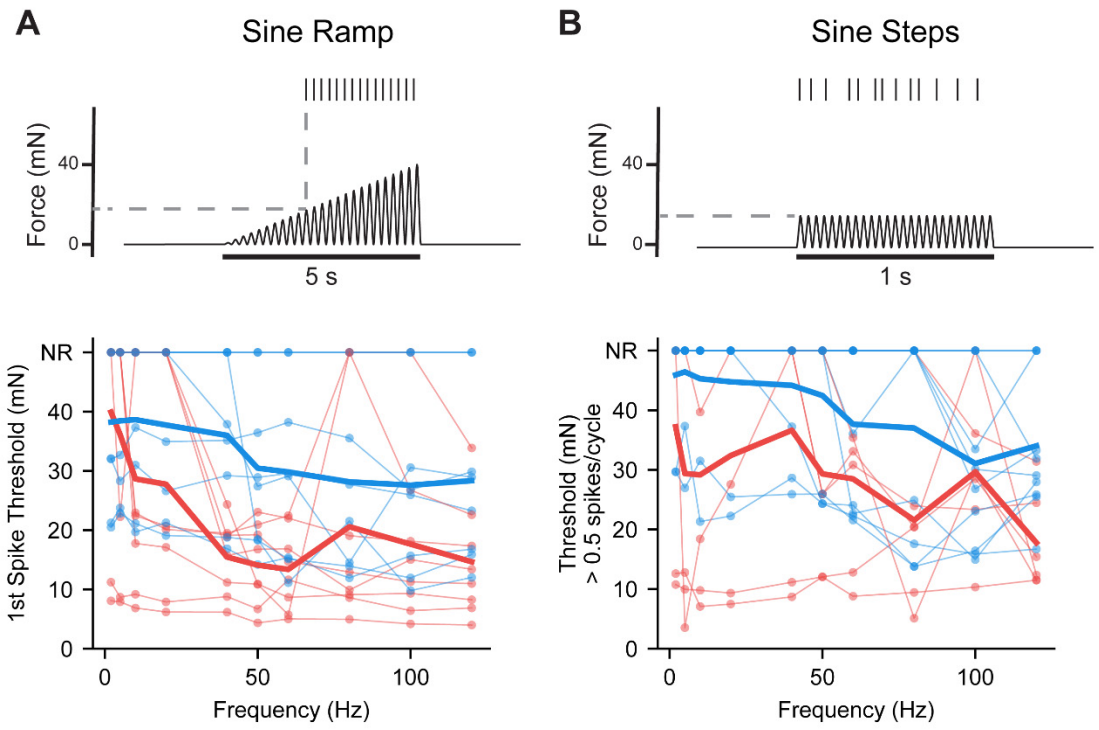

Fig. S8. TrkB$^+$ and Ret$^+$ Meissner afferents exhibit a wide range of frequency tuning to 2-120 Hz sinusoidal vibrations.

A. Top: Schematic of threshold determination to intensity-ramping sine stimuli. The threshold was measured as the force of the sine envelope at the time of the first action potential. Bottom: thresholds for individual (connected points) and mean (thick line) TrkB$^+$ (blue) and Ret$^+$ (red) Meissner afferents. NR: no response.

B. Top: Schematic of threshold determination to a sine-step protocol. Intensities and frequencies were drawn at random, and the intensity at which the Meissner afferent fired greater than 0.5 spikes/cycle was considered the threshold for each frequency. Bottom: thresholds for individual (connected points) and mean (thick line) TrkB+ (blue) and Ret+ (red) Meissner afferents. NR: no response.

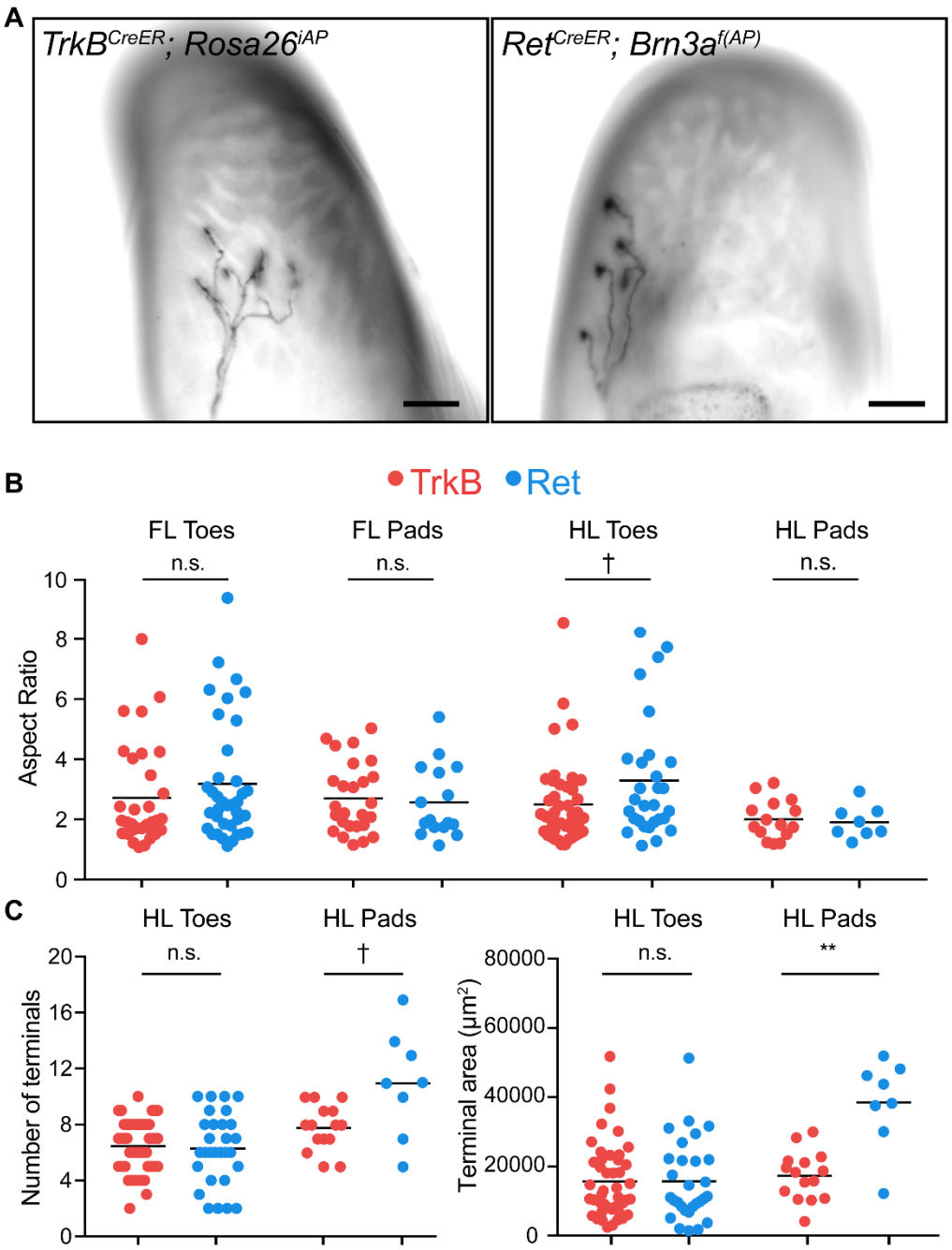

Fig. S9. Measurements of TrkB⁺ and Ret⁺ Meissner afferent morphological receptive fields.

A. Representative images of whole-mount, AP-stained digital pads of a *TrkB^{CreER}; Rosa26^{iAP}* mouse (left) and a *Ret^{CreER}; Brn3a$^{f(AP)}$* mouse (right), in which TrkB⁺ and Ret⁺ Meissner afferents were sparsely labeled using a low dose of tamoxifen, respectively. Images depict individual

Meissner corpuscle afferents innervating glabrous digital pads. Analysis includes a total 119 individual TrkB^{+} afferent receptive fields (58 forelimb and 61 hindlimb) from 21 mice for and a total of 90 individual Ret^{+} afferent receptive fields (53 forelimb and 37 hindlimb) from 21 mice. (scale bars = 100 µm)

B-C. Aspect ratios (B, major axis/minor axis), number of terminal endings (C, left), and surface areas (C, right) of TrkB^{+} and Ret^{+} Meissner afferent morphological receptive fields measured in *TrkB^{CreER}; Rosa26^{iAP}* or *TrkB^{CreER}; Brn3a$^{f(AP)}$* mice and *Ret^{CreER}; Rosa26^{iAP}* or *Ret^{CreER}; Brn3a$^{f(AP)}$* mice. Individual measurements and mean values (black bar) are plotted for each group. Receptive field quantification plotted here and in Figure 3 includes data from 119 individual TrkB^{+} afferent receptive fields (58 forelimb and 61 hindlimb) from 21 mice and from 90 individual Ret^{+} afferent receptive fields (37 hindlimb and 53 forelimb) from 21 mice. (two-tailed Welch's t-test, mean significantly different: ** $p < .01$; F-test of the equality of variances, variance significantly different: † $p < .05$).

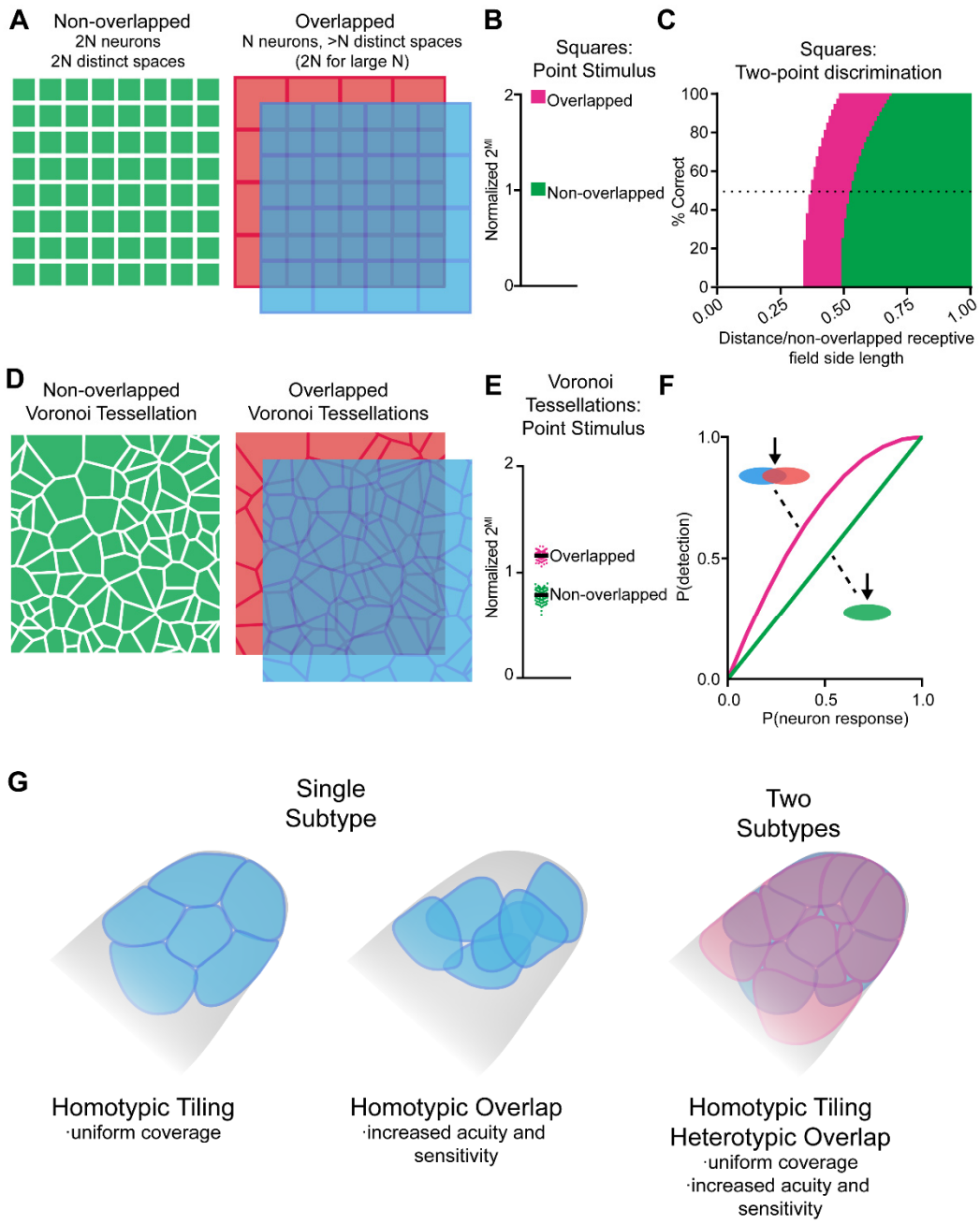

Fig. S10. Computational modeling suggests that heterotypic overlap of homotypically tiled mosaics, like that observed in Meissner corpuscle afferents, enables both uniform skin coverage and enhanced acuity.

A. Schematic demonstrating overlapped grids of homotypically tiled uniform squares (blue and red) and their equivalent non-overlapped grids (green). Overlapped receptive fields provide

greater than N discriminable spaces (approaching 2N for large numbers of neurons), while non-overlapped receptive fields would require more neurons with smaller receptive fields to achieve the same resolution (see Methods).

B. Mutual information (MI) between a single pixel stimulus and the responses of simulated grids of uniform squares with overlapped and non-overlapped arrangements. Mutual information was normalized by the number of neurons ($2^{MI}/N$) such that perfect performance of a non-overlapped arrangement should be equal to 1 and perfect performance for an overlapped arrangement should be 2 (see Methods).

C. Two-point discrimination ability of overlapped vs. non-overlapped grids. The two stimuli were 1) a central point and 2) a point shifted by some distance from the central point. For each distance, the point was positioned at all angles between 0 and 2π radians. The percentage of points in which the representation of the central point and the representation of the shifted point were different are plotted for each distance relative to the side lengths of the square neurons of the non-overlapped arrangement (see Methods). For a fair comparison, modeled receptive fields for the overlapped arrangement are larger than for the non-overlapped arrangement to achieve the same total number of neurons.

D. Schematic of non-overlapped (left) and overlapped (right) Voronoi tessellations.

E. Mutual information ($2^{MI}/N$) between a single point stimulus and the responses of overlapped and non-overlapped Voronoi tessellations generated in MATLAB (see Methods for details). Using 4000 generated tessellations, pairs of tessellations were overlapped to create 2000 overlapped mosaics. The number of neurons, N, was the number of randomly seeded points per arrangement, and MI was normalized by N to allow comparison between arrangements

with different numbers of neurons. A random subset of these results is plotted: The pink circles represent the normalized MI for 100 examples of overlapped tessellations, and the green circles represent the normalized MI for 100 examples of non-overlapped tessellations. Black bars in both cases represent the overall mean.

F. Probability of detection (the probability that at least one neuron responds) plotted as a function of the probability of a single neuron responding to a stimulus within its receptive field. The green line depicts the probability of detection for a single-layered arrangement of homotypically tiled neurons (P(neuron responds)). The pink line indicates the probability of detection for a double-layered arrangement of overlapping neurons assuming the neurons are independent ($1-(1-P(\text{neuron responds}))^2$). The probability of detection is greater for an overlapping arrangement at all probabilities between 0 and 1, exclusive.

G. Homotypic tiling of a single subtype of Meissner tactile afferents ensures uniform and complete coverage of the skin surface (left). On the other hand, homotypic overlap can provide higher sensitivity and acuity, but this arrangement comes at the expense of the uniformity and completeness of skin coverage ensured by a tiling mechanism (center). Combining both homotypic tiling and non-redundant heterotypic overlap through the existence of two molecularly distinct subtypes of tactile afferents ensures uniform and complete coverage of the skin while also enabling high acuity and sensitivity, using the fewest neurons (right).

Movie S1

Advillin^{Cre};TrkB$^{flox/+}$ (control) mouse demonstrating typical sunflower seed eating behavior.

Movie S2

TrkB^{cKO} mouse demonstrating difficulty with opening and eating sunflower seeds.